Spatiotemporal variability of pH and carbonate parameters on the Canadian Atlantic Continental Shelf between 2014 and 2022

Olivia Gibb[1], Frédéric Cyr[1], Kumiko Azetsu-Scott[2], Joël Chassé[3], Darlene Childs[2], Carrie-Ellen Gabriel[2], Peter S. Galbraith[4], Gary Maillet[1], Pierre Pepin[1], Stephen Punshon[2], and Michel Starr[4]

[1]Northwest Atlantic Fisheries Centre, Fisheries and Oceans Canada, St. John's, NL, Canada
[2]Bedford Institute of Oceanography, Fisheries and Oceans Canada, Dartmouth, NS, Canada
[3]Gulf Fisheries Centre, Fisheries and Oceans Canada, Moncton, NB, Canada
[4]Maurice Lamontagne Institute, Fisheries and Oceans Canada, Mont-Joli, QC, Canada

Correspondence: Frédéric Cyr (Frederic.Cyr@dfo-mpo.gc.ca)

Abstract. The Atlantic Zone Monitoring Program (AZMP) was established by Fisheries and Oceans Canada (DFO) in 1998 with the aim of monitoring physical and biological ocean conditions in Atlantic Canada in support of fisheries management. Since 2014, at least two of the carbonate parameters (pH, Total Alkalinity - TA, Dissolved Inorganic Carbon - DIC) have also been systematically measured as part of the AZMP, enabling the calculation of derived parameters (e.g., carbonate saturation states - Ω, partial pressure of CO_2 - pCO_2, etc.). The present study gives an overview of the spatiotemporal variability of these parameters between 2014 and 2022. Results show that the variability of the carbonate system reflects changes in both physical (e.g., temperature, salinity) and biological (e.g., plankton photosynthesis and respiration) parameters. For example, most of the region undergoes a seasonal warming and freshening. While the former will tend to increase Ω, the latter will decrease both TA and Ω. Spring and summer plankton blooms decrease DIC near the surface and then remineralize and increase DIC at depth in the fall. The lowest pCO_2 values (down to $\sim$200 μatm) are located in the cold Coastal Labrador Current and the highest (>1500 μatm) in the fresh waters of the Gulf of St. Lawrence and the St. Lawrence Estuary. The latter is also the host of the lowest pH values of the zone (7.48 in the fall of 2022). Finally, most of the bottom waters of the Gulf of St. Lawrence (>90%) are undersaturated with respect to aragonite (Ω_{arg}<1). In addition to providing a baseline of carbonate parameters of the Atlantic Zone as a whole, this comprehensive overview is a necessary and useful contribution for the modeling community and for more in-depth studies. The full dataset of measured and derived parameters is available in the Federated Research Data Repository at https://doi.org/10.20383/102.0673.

1 Introduction

The Canadian Atlantic continental shelf and slope, termed the Canadian Atlantic Zone (or simply Atlantic Zone hereafter), is at the confluence of waters of contrasting origins (Figure 1). The northward flowing warm and saline Gulf Stream, the southward flowing cold less saline Labrador Current, and the fresh outflow from the St. Lawrence River and the Gulf of St. Lawrence provide a unique range in salinities and temperatures (Figure 2a) which form oceanic fronts along the shelf-slope edge sur-

rounding the Atlantic Zone (Belkin et al., 2009; Cyr and Larouche, 2015). These fronts are often associated with vertical nutrient transport, high productivity and ecological hot spots with a rich diversity and abundance of organisms (e.g. Lévy et al., 2012). As a result, the Atlantic Zone supports a variety of commercially important species which amounted to nearly 5 billion
25   dollars (\$G) in commercial landings (\$4.2G) and finfish and shellfish aquaculture (\$0.6G) in 2021 (DFO, 2022). These ecosystems however are becoming stressed due to changes to the physical, chemical, and biological oceanographic environment as a result industrialization, e.g., burning of fossil fuels, agriculture, deforestation (Bernier et al., 2018; Doney, 2010). Increasing atmospheric carbon dioxide (CO_2) concentrations not only increases atmospheric and sea surface temperatures but alters the ocean's carbonate cycle resulting in increased ocean acidity (i.e. decreased pH). Many aquatic species within the Atlantic Zone
30   are vulnerable to the effects of ocean acidification, which may affect the entire ecosystem (Fabry et al., 2008; Doney, 2010). Calcifying shellfish are directly impacted by ocean acidification while other shellfish and finfish can be indirectly impacted (Kroeker et al., 2013). The socioeconomic impacts of ocean acidification and climate change on fisheries (e.g., resources decline, changes in species distribution, income and cultural losses, etc.) have been assessed for various ecosystems (Cooley and Doney, 2009; Mathis et al., 2015; Wilson et al., 2020). Monitoring the physical, chemical and biological oceanographic
35   conditions and determining a baseline is required prior to an assessment of future aquaculture and fisheries in the Atlantic Zone.

     Implemented in 1998 by Fisheries and Oceans Canada (DFO), the Atlantic Zone Monitoring Program (AZMP) was designed to evaluate the physical (temperature, salinity), chemical (nutrients and dissolved oxygen concentrations), and biological (chlorophyll-a, fluorescence, plankton species assemblage and abundance) oceanographic properties of the Canadian
40   Northwest Atlantic (Therriault et al., 1998). The AZMP characterizes the spatial and temporal (seasonal to decadal) variability of these oceanic properties. It is carried out by the four Atlantic DFO administration centers (three geographic regions): Quebec/Gulf, Maritimes and Newfoundland and Labrador (Figure 3). The AZMP annually publishes a summary of oceanographic conditions that assesses the current state of the ecosystem. It is used for stock assessments and marine resource management by DFO, and supports fundamental oceanographic research. In fall 2014, the sampling and analysis of two of the carbonate
45   parameters, including total alkalinity (TA), total dissolved inorganic carbon (DIC), and pH were added to the AZMP mandate. The resulting dataset is the focus of the present paper.

     Ocean acidification is the decrease in ocean pH (increase in H^+, acidity) and carbonate ion concentration (CO_3^{2-}) due to the increased uptake of anthropogenic CO_2 (Millero, 2007). Seawater carbonate chemistry involves the dissolution of atmospheric CO_2 (Eq. 1), acid/base reactions forming the inorganic carbonate (DIC) species in equation (Eq. 2), and the formation and
50   dissolution of solid calcium carbonate ($CaCO_3$) (Eq. 3).

$$CO_{2_{atm}} \rightleftharpoons CO_{2_{aq}} \tag{1}$$

$$CO_{2_{aq}} + H_2O \rightleftharpoons H^+ + HCO_3^-$$
$$HCO_3^- \rightleftharpoons H^+ + CO_3^{2-} \tag{2}$$

$$CaCO_3 \rightleftharpoons \left[Ca^{2+}\right] + \left[CO_3^{2-}\right] \tag{3}$$

The photosynthesis and respiration of organic matter is another factor that contributes to changes in the carbonate system

55 (Eq. 4). Spring phytoplankton blooms increase surface water pH by consuming CO_2 in water, while at depth the remineralization of that vertically exported organic matter to DIC lowers pH.

$$CH_2O + O_2 \rightleftharpoons CO_2 + H_2O \tag{4}$$

The degree in which seawater is saturated with calcium carbonate ($CaCO_3$) is known as the $CaCO_3$ saturation state (Ω). The saturation state is a function of calcium and carbonate concentrations, and its apparent solubility product (K_{sp}^*) which is a

60 function of temperature, salinity and pressure (Mucci, 1983; Millero, 1995):

$$\Omega = \frac{\left[Ca^{2+}\right]\left[CO_3^{2-}\right]}{K_{sp}^*}. \tag{5}$$

Seawater with an $\Omega > 1$ is considered oversaturated which induces carbonate precipitation, while water with $\Omega < 1$ is considered undersaturated and corrosive which promotes carbonate dissolution. The carbonate saturation state customarily decreases with depth as a result of cold temperatures, increased pressure, and respired DIC. The depth at which the water becomes un-

65 dersaturated is generally referred to as *saturation horizon*. Organisms such as phytoplankton, zooplankton and invertebrates (clams, oysters, corals) that form shells and skeletons of calcium carbonate ($CaCO_3$) may have difficulty maintaining or forming hard structures in undersaturated waters. It should be noted, however, several studies have identified higher critical thresholds ($\Omega \sim 1.3-2$) for marine organisms (e.g., Ekstrom et al., 2015; Waldbusser et al., 2015; Siedlecki et al., 2021). The two most common forms of $CaCO_3$ are calcite and aragonite. Because aragonite is more soluble than calcite, the aragonite

70 saturation horizon (Ω=1) is shallower, and organisms that produce aragonite may be more vulnerable to a decreasing saturation state as atmospheric CO_2 increases.

Freshwater influx also plays an important role on the carbonate system. The freshwater effects on Ω is due to both changes in DIC/TA ratio in source waters, and to the decrease in Ca^+ concentration as a function of salinity (e.g Azetsu-Scott et al., 2014; Hunt et al., 2021). TA is an indicator of seawater's ability to buffer (neutralize) acids. It is a measure of the excess total proton

75 acceptors (anions) over proton donors (acids) formed by dissociation of carbonic, boric, and other weak acids in seawater. It is expressed as mole equivalents of hydrogen ions per kilogram of seawater. Therefore, TA will decrease with freshwater influx and during carbonate precipitation (decrease in DIC), which will subsequently decrease Ω:

$$CO_2 + CaCO_3 + H_2O \rightleftharpoons 2HCO_3^- + Ca^{2+}. \tag{6}$$
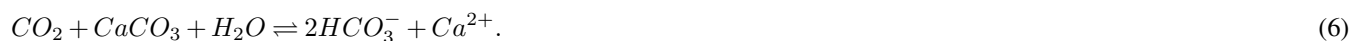
2 Physical Oceanographic setting

80   The physical properties of the Atlantic Zone are dominated by large-scale interactions of Arctic, sub-polar and sub-tropical waters and fresh water influx from the St. Lawrence river (e.g., Loder et al., 1998; Han et al., 2008; Brickman et al., 2016). The geographic and current names described below are shown in Figure 1, and the different water masses (or water origin) of this system are loosely highlighted in a temperature vs salinity (T-S) and depth plot of the entire dataset (Figure 2a). The two major circulation features are the southward flowing Labrador Current, which brings cold and less saline subpolar waters

85   along the NL shelf, and the northeastward flowing Gulf Stream (with the North Atlantic Current, NAC, its northeast extension) which carries warm and saline sub-tropical waters along the Scotian Shelf and the Grand Banks. The latter is labeled North Atlantic Waters, NAtlW, in Figure 2. An additional input of Arctic-origin cooler and fresher waters also flows on the inshore part of the Newfoundland and Labrador Shelf, a current generally referred to as the Inshore Labrador Current, or Labrador Coastal Current (Florindo-López et al., 2020). These contrasting water masses interact on the shelf and partially enter the Gulf

90   of St. Lawrence (GSL), a semi-enclosed basin characterized by an estuarine circulation.

On the Scotian Shelf, Slope Waters that lie along the shelf break are a combination of cold, less saline, oxygen-rich and nutrient-poor Labrador Slope Water (LSW) from the Labrador Current, and warm and saline, nutrient-rich and oxygen-poor Warm Slope Water (WSW) derived from the NAC. The properties of the Slope Water vary depending on which component (LSW vs WSW) is dominant (Petrie and Drinkwater, 1993). This mixture is advected inland in the deep waters of the Laurentian

95   Channel by the estuarine circulation of the GSL. As these waters flow landward toward the Lower St. Lawrence Estuary (LSLE), oxygen is consumed and the deep water becomes hypoxic (Gilbert et al., 2005). These low oxygen concentrations have been associated with increased composition ratio of WSW relative to LSW (Gilbert et al., 2005; Jutras et al., 2020), poor ventilation (>16 years, Mucci et al., 2011) and increased oxygen demand in bottom waters because of respiration and remineralization of organic matter supplied by increased primary productivity at surface (Thibodeau et al., 2006). The Scotian

100   Shelf Water receives subpolar water primarily from the GSL through western Cabot Strait, and a smaller portion directly from the Newfoundland Shelf by the Labrador Current across the Laurentian Channel (Dever et al., 2016).

In the summer, the water column of the Atlantic Zone is generally characterised by a three-layer system. A seasonally warmed thin and relatively fresh surface layer overlies a cold intermediate layer (CIL), which is the remnant of the previous winter cold surface layer. A warmer, more saline slope-derived water lies below the CIL. The deeper waters (>200 m) are

105   generally limited to channels and troughs, and there are areas (e.g. southwestern Scotian Shelf) where the CIL is absent due to mixing. In the late fall and winter, the surface water cools, deepens and combines with the CIL into a two-layer system. In places, this winter mixed layer reaches the freezing point and sea ice is formed. This winter layer is at the origin of the following summer CIL (Galbraith, 2006).

The Atlantic Zone is thus characterized by a large range of temperatures (freezing point to over 25°C during the summer)

110   and salinities (freshwater to over 37), which influences the carbonate system as discussed later. The Atlantic Zone is divided here into three regions geographically and then further using bathymetrical considerations: shelf (fresher) versus slope (more saline), surface (warm in summer) versus subsurface (cool).

3 Sampling and Methodology

The dataset presented here consist of carbonate parameters compiled from multiple surveys from all four administrative AZMP
Regions: Newfoundland and Labrador (NL), Maritimes (MAR), Québec (QC) and Gulf. The latter two sample the GSL Region
and will be combined under this name herein (e.g., Fig. 3). The map of the Atlantic Zone in Figure 3a shows the locations
of the standard AZMP sections, as well as two sections through the GSL established here to plot depth profiles across (GSL;
from the Magdalen Shallows on the southwest to the strait of Belle Isle in the northeast) and along the Laurentian Channel
(LC; the deep channel that runs from Cabot strait to the head of the LSLE), shown magnified in Figure 3b. For the purpose
of presenting the data, the Cabot Strait Line (CSL) will be associated with the GSL. Unless explicitly stated, the waters of
the Upper St. Lawrence Estuary (USLE) and the Saguenay Fjord (SF; Figure 3b), are not discussed in this study because
their properties, highly influenced by freshwater input, are very different than the rest of the Atlantic Zone. These data are
however included in the dataset that accompanies this paper. All bathymetric maps were generated using the GEBCO 2014
Grid bathymetry product, version 20150318, http://www.gebco.net (consulted 10 April 2019).

3.1 Sampling

Carbonate chemistry data have been sampled in the Atlantic Zone since the fall of 2014 (except for high frequency station
Rimouski where the sampling started earlier, see below). Depending on the region, between two to three surveys usually occur
every year since. An overview of all missions, their dates and the parameter sampled is provided in Table 1.

The NL Region, due to its extensive shelf/slope spatial extent, is scheduled to survey the NL Shelf and Slope three times a
year, generally from section Southwest St. Pierre Bank (SWSPB) up to the northern sea ice extent, usually section Bonavista
Bay (BB), during spring (April) surveys, from section Flemish Cap (FC) to Beachy Island (BI) during summer (July) surveys,
and from section SWSPB to Seal Island (SI) during fall (November) surveys (Figure 3a). The surveys are most often incomplete
due to operational constraints caused by sea ice, weather or research vessel downtime. The NL Region aims to sample at surface
(∼5 m), 10, 50, 75, 100, 150, 250, 500, 1000 m and bottom. Sampling down the shelf slope to depths greater than 1200 m was
however only feasible during fall surveys (maximum 3677 m) because of limited vessel capacity during other seasons.

The Maritimes Region has a spring (April) and a fall (September/October, except November/December in 2017) survey
which were consistently sampled between 2014 and 2022 (Figure 3a). The Scotian Shelf and Slope were sampled at surface
(∼2 m), 10, 50, 80, 100, 150, 250, 500, 1000, 1500 m and bottom.

The GSL is sampled during spring (June) and fall (October/November) surveys along the standard sections at surface (∼2 m),
15, 50, 100, 150, 200, 300, 400 m and bottom (Figure 3b). Samples are also acquired during groundfish surveys in the GSL (Figure 3b, Table 1) during summer (August/September) 2017-2022 (Trip_Name: 'IML2017027', 'PER2017018', 'PER2017024',
'PER2017016', 'PER2017026', MLB2017001b', 'IML201841', 'PER2018041', 'PER2018042', 'PER2018043', 'TEL2018196'
IML2019036', 'PER2019140', 'PER2019008', 'TEL2019201', 'PER2020019', 'PER2021156', 'PER2021151', 'CJC2021222',
'IML2021030', 'PER2021021', 'IML2022039', 'PER2022022', 'CAR2022025', 'PER202223330'). Although these surveys

are not within the regular AZMP program, they are staffed by the AZMP for oceanographic sampling and provide extensive spatial and added temporal (summer) coverage of carbonate parameters of the GSL.

The fall 2014 and spring 2017 AZMP surveys had the most complete spatial coverage of the Atlantic Zone among the entire time series. The other surveys are partial due to operational limitations specific to each region (see Table 1 for the timing of the different surveys per Region).

In addition, two coastal stations are sampled at a greater temporal frequency. Rimouski Station (labeled "Rimouski" in Figures 1 and 3) located in the LSLE is sampled by the Quebec Region on a near-weekly basis. Station 27 (labeled "STN27" in Figures 1 and 3), located on the path of the Labrador coastal current just outside St. John's harbour is sampled by the NL Region on a near-monthly basis. To illustrate their respective temporal coverage, the time series of pH at these stations (measured at Rimouski Station and derived from TA/DIC at Station 27) are presented in Figure 4. Note that Rimouski Station is the only time series starting in the spring of 2014 in this dataset (all other sampling starts in the fall of 2014).

The collection of discrete water samples for carbonate analyses was achieved using a 12 or 24 Niskin bottles rosette equipped with a SeaBird Conductivity-Temperature-Depth (CTD) coupled with an oxygen sensor to continuously measure depth, temperature, salinity and dissolved oxygen concentration (DO). Aliquots of water were subsampled from each Niskin bottle for nutrients (PO_4, SiO_3, $NO_3 + NO_2$) and DO, then processed and analysed according to established standard protocols (Mitchell et al., 2002). Although the DO concentration ($mL\,L^{-1}$) is available with this dataset, it was sampled less frequently than the other oceanographic parameters because its purpose is to calibrate the DO sensor measurements. The GSL Region sampled DO at the surface and bottom, and the MAR region sampled DO at surface, bottom and mid-depth of the water column. The NL region sampled DO at all depths, but at a subsampled number of stations (roughly every 2 to 4 stations along a section). GSL and NL Regions used their subset of bottle DO values to calibrate their DO sensor on the CTD providing a DO value for each sample bottle (even when no Winkler titration was realized). For MAR data, only DO data obtained from Winkler titration are provided. Oxygen saturation ($O_{2_{sat}}$) in % was calculated as the ratio between the measured DO concentration and its solubility referenced to surface using the TEOS-10 toolbox (McDougall and Barker, 2011) and corresponding T-S observations.

Aliquots of water for the analysis of pH, total alkalinity (TA) and total dissolved inorganic carbon (DIC) (or combination thereof) were subsampled following protocols established by Dickson et al. (2007). Each aliquot was carefully drawn from the Niskin bottles, transferred into 500 mL gas-tight borosilicate reagent bottles (Corning, USA), and allowed to overflow by one volume while precluding air bubbles. A 5 mL volume was then removed to create a headspace for thermal expansion. The samples were preserved with 100 μL of saturated $HgCl_2$ to prevent further biological activity. Each bottle was sealed with a ground-glass stopper, high-vacuum (Apiezon M) grease, and a rubber band then stored in the dark between 4 and 18°C for up to 6 months prior to analysis.

3.2 Analytical methods – carbonate parameters

In 2014, the first year of the program, all three carbonate parameters (pH, TA, DIC) were analysed by the Maritimes Region at the Bedford Institute of Oceanography (BIO, Dartmouth NS). In subsequent years, the GSL region analysed TA and pH at the Maurice Lamontagne Institute (MLI, Mont-Joli QC), added DIC in fall 2019, and only measured pH in the spring of 2015

(Trip_Name 'IML201516'). After 2014, the Maritimes (BIO) and NL (Northwest Atlantic Fisheries Centre - NAFC, St. John's
NL) Regions analysed TA and DIC within their respective facilities. An overview of the carbonate parameters measured during
each mission is provided in Table 1.

DIC (in $\mu mol\,kg^{-1}$ of seawater) is extracted as CO_2 by purging an acidified (1M, 8.5% phosphoric acid in excess) aliquot
of water (warmed to 25°C) with ultra-high purity (UHP) nitrogen gas using an automated sampling and gas extraction system.
The dried gas, including the CO_2, is transferred and absorbed into a coulometric cell and analysed by titration and photometric
detection (Johnson et al., 1993). Various makes and models of autosamplers and analyzers were used by the different regions.
Duplicate or triplicate sample measurements provided an analytical precision of 0.03% at BIO and < 0.1% at IML and NAFC.

TA (in $\mu mol\,kg^{-1}$ of seawater) was measured by open-cell potentiometric titration (Dickson et al., 2007; Mintrop et al.,
2000) with an automated sampling system. Each 50 (NAFC/BIO) or 104 (IML) mL sample, warmed to 25°C, is titrated with
0.1 M hydrochloric acid to the Gran equivalence point (non-linear curve fit method) using a computer controlled Dosimat
(Metrohm AG) dispenser and combination glass electrode. In the NL Region, aliquots of 0.1M hydrochloric acid are added in
a 25°C thermostated jacket open cell while gently mixing the sample, and pH measurements are allowed to stabilize between
successive readings. The analytical precision of TA at BIO was calculated using repeat analyses of bulk seawater and reported
as ±0.05%, while duplicate sample analyses revealed a precision of < 0.1% at IML and NAFC.

Seawater pH expressed in the total hydrogen ion scale (pH_T) was determined by spectrophotometry and calculated following
the equations with dye perturbation (Clayton and Byrne, 1993; Dickson et al., 2007). Purified m-cresol purple solution (University of South Florida) was added to seawater held at $25 \pm 0.05°C$ in a 10 cm path-length quartz cell and mixed thoroughly.
The ratio of blank-corrected absorbances measured at 434, 578 and 730 nm with a spectrophotometer (Agilent Technologies,
USA) was used to determine pH_T. pH measurements are not corrected for dye perturbation, but the m-cresol dye is visually
inspected each day and measurements are made to ensure its stability over time. Precision and accuracy, evaluated daily by
repeat measurements of a tris(hydroxymethyl)aminomethane (TRIS) buffer solution (A.G. Dickson, Scripps Oceanographic
Institution, San Diego, CA) prepared with a salinity of 30 (Millero, 1986), were typically ±0.002 pH units at BIO and ±0.003
pH units or better at IML.

All analytical methods were calibrated with a series of seawater certified reference materials (CRM; A.G. Dickson, Scripps
Institute of Oceanography, San Diego, CA), which allowed for performance evaluations of the various instruments and to
normalize the TIC, TA and pH measurements. Since the analyses were conducted at three different regions, we will consider
the largest analytical error provided for all measurements: TA and DIC values will be $\pm 0.1\,\%$ or $\pm 2.1\,\mu mol\,kg^{-1}$, and pH will
be ±0.003 units. These uncertainties are comparable to those suggested by Dickson (2010) for modern analytical techniques
using reference materials. All data flagged as suspect because of analytical error by each laboratory have been removed from
the dataset.

3.3 Calculation of carbonate parameters

The aragonite saturation state (Ω_{arg}), calcite saturation state (Ω_{cal}; in dataset but not discussed in this report), $pH_{T,is}$ (total
scale, in situ) and the partial pressure of CO_2 (pCO_2 in μatm) were calculated using the CO2SYS program (Lewis and

Wallace, 1998) modified for Python (Humphreys et al., 2020, https:github.commvdh7PyCO2SYStreev1.2.1) as recommended for "best practices" by Orr et al. (2015). The dissociation constants (K_1, K_2) of Mehrbach et al. (1973) as refit by Dickson and Millero (1987) (Mdm), total boron constant from (Uppstrom, 1974), and KHSO$_4$ constant from Dickson (1990) were also used as recommended for "best-practices" (Chen et al., 2015; Dickson et al., 2007; Orr et al., 2015). Although it has been suggested that dissociation constants formulated for estuarine waters (Cai and Wang, 1998; Millero, 2010) should be used to avoid differences in the calculation of carbonate parameters at low salinity (Dinauer and Mucci, 2017), there is some evidence that formulations other than those for "best practices" may produce discrepancies (Orr et al., 2015; Dinauer and Mucci, 2018). The dissociation constants by Mdm were formulated for salinities > 20. Samples with salinities < 20 constitute only 0.15% of this dataset (1% of the data from the GSL), and the differences in calculated carbonate parameters using the constants by Cai and Wang (1998) and Mdm are approximately double for samples with salinity $\geq$20 than those <20 (Table 2a). Therefore, the dissociation constants by Mdm were used in order to avoid discrepancies to the other 99.85% of the dataset. The chosen combination of constants listed above was also suggested by Raimondi et al. (2019) because they generated the best internal consistency in their Labrador Sea (AR7W) dataset. However, their choice of constants provided less uncertainty than their choice of input parameters. The carbonate parameters in this dataset were calculated using the TA (μmol kg^{-1}seawater, or SW) provided by all regions and either DIC (μmol kg^{-1} SW) or pH_T, which is region dependent. According to the results by Raimondi et al. (2019), the TA/DIC based calculations of pH (e.g., NL and MAR Regions) produce low accuracy yet low uncertainty, and the TA/pH based calculations of DIC (e.g., GSL dataset) provide the best consistency. The TA/pH pair will thus be used for calculating pCO$_2$ when both pH and DIC were collected in addition to TA (see Table 1). Since the GSL region consistently measures the three carbonate equilibria parameters since the fall of 2019 (TA, pH and DIC; see Table 1), we estimated the variability of the other derived parameters (pH in situ, Ω, pCO$_2$) using the different combination of pairs for this region between 2019 and 2020, as well as for 2022 (in 2021, only TA and pH were measured). Results are presented in Table 2d and discussed later in the text.

The spring 2015 GSL dataset (Trip_Name 'IML201516') consists solely of pH data (in vitro at 25°C). In order to obtain in situ values and other carbonate parameters, TA was estimated using the TA-salinity linear relationship (Cai et al., 2010; Fassbender et al., 2017) for S>20. Using spring data at all depths and remaining years in the GSL (excluding the high resolution Rimouski station data), this led to the fit: TA = 43.09 x S + 808.31 ($r^2 = 0.98$, $p < 0.001$; see Figure 5b). The estimated freshwater TA end-member (S=0) is 808.31 μmol kg^{-1}. This value is lower than the measured values of $1204\pm99\,\mu$mol kg^{-1}or $1081 \pm 30.2\,\mu$mol kg^{-1}by Dinauer and Mucci (2017, 2018) near Québec City, and the $1000\,\mu$mol kg^{-1}measured by Mucci et al. (2017) west of the Saguenay Fjord. It is however higher than $186\,\mu$mol kg^{-1}calculated by Dinauer and Mucci (2018) as a measure of the Saguenay Fjord and North Shore Rivers, and $80\,\mu$mol kg^{-1}in the Saguenay River measured by Mucci et al. (2017). Using a localised dataset for this calculation accounted for the low salinity water exiting the St. Lawrence River. Considering the measurement error of up to 0.1%, there was no significant difference in the predicted TA between the spring dataset and all seasons in the GSL. To estimate the degree in which the predicted TA had an effect on the calculation of the other carbonate parameters, the parameters for the spring 2015 GSL dataset were calculated in CO2SYS (TA/pH) with the

maximum and minimum values of TA $\pm$ 2 SD ($1.28\,\mu mol\,kg^{-1}$), the TA-salinity regression uncertainty. This exercise shows the low sensitivity of this method with error less than 0.03% (Table 2*c*).

The calculated carbonate parameters were calibrated to in situ conditions using temperature (°C), salinity (psu) and pressure (dbar). The nutrient alkalinity, which is represented by total soluble reactive phosphorus (PO_4, $\mu mol\,kg^{-1}$ SW) and total soluble reactive silicate (SiO_3, $\mu mol\,kg^{-1}$ SW), were used as additional parameters when available since they contribute to the calculation of the total carbonate alkalinity (Orr et al., 2015). There can be a slight offset in calculated carbonate parameters when the nutrient data are absent, especially in high concentration regions. This offset has been calculated for the Atlantic Zone by obtaining the difference in carbonate parameters calculated with and without nutrients (nutrients set to zero in CO2SYS; Fassbender et al., 2017). The calculation was performed on two datasets: the TA/DIC input pair from the NL and MAR regions and the TA/pH input pair from the GSL region. The results (Table 2*b*) indicate that all calculated carbonate parameters except for pCO_2 will be slightly higher when nutrient data are lacking, with TA/DIC as input pair having the largest offset. The difference in calculated pH (0.002 pH units) and DIC ($1.02\,\mu mol\,kg^{-1}$) values are below the analytical uncertainty (± 0.005 pH units, $\pm 2.1\,\mu mol\,kg^{-1}$, respectively). The mean saturation states and pCO_2 have changed by < 0.6% for the TA/DIC pair and < 0.1% for the TA/pH pair. The larger nutrient-no nutrient difference with the TA/DIC pair may be due to the higher nutrient concentrations in the GSL Region (> $17.3\mu M$ PO_4, > $49.1\mu M$ SiO_3), or reflecting the input parameter propagated error as suggested by Raimondi et al. (2019) as well as by Dickson (2010) who estimated the uncertainty in calculating the saturation state with 3.7% error using the TA/pH pair relative to 1.7% with TA/DIC.

The entire dataset used here is however provided for follow up studies (see Data Availability section). This dataset includes the following physical, biogeochemical, and carbonate parameters: temperature (T), salinity (S), dissolved oxygen concentration (DO), oxygen saturation ($O_{2_{sat}}$), nutrient data (PO_4, SiO_3, $NO_3 + NO_2$), measured and calculated (same as measured when available) TA and DIC, measured pH in the laboratory (when available), and calculated *in situ* pH, pCO_2, Ω_{arg}, and Ω_{cal}.

4   Results and Discussion

In the Atlantic Zone, the spatial and temporal variability of carbonate parameters reflects changes in both physical (temperature, salinity) and biological (plankton photosynthesis and respiration) parameters. While a complete description of the seasonal variability of the Atlantic zone is difficult due to the timing of the surveys and large geographic areas of all three regions, some general description can be drawn.

In the following subsections, a summary of the physical and carbonate parameters is presented for different regions, seasons and depth range. Here surface is defined as the shallowest sample, but no deeper than 52 m (a depth chosen to encompass sampling variations around the targeted 50 m depth), and bottom as the deepest sample below 50 m. Due to some instances where near-bottom samples were not achieved (>1200m areas due to ship limitation, e.g. NL slope), the following descriptions are restricted to depth shallower than 600 m. All of the data are however in the dataset.

A subset of the data (excluding nutrients and O_2) is presented in Appendix A on maps of the surface and bottom waters of the Atlantic Zone for each sampling season of 2017, the most extensively sampled year to date (Figures A1-A9). Each map

represents one variable per depth per season. Seasons are defined as spring (beginning of March to end of June), summer (beginning of July to September 14th), and fall (September 15th to end of December). The fall 2017 maps are presented in Figures 6 to 8.

Depth profiles along a series of hydrographic sections from each region during the fall of 2017 are presented in Appendix B for the same set of variables. These sections include Seal Island (SI; Figure A10), Flemish Cap (FC; Figure A11), Halifax (HL; Figure A12), Cabot Strait (CSL; Figure A13), and Laurentian Channel (LC; Figure A14) which is the line of stations from the centre of the Lower St. Lawrence Estuary through the Laurentian Channel to Cabot Strait (Figure 3a). The results will be discussed as they are introduced.

4.1 Oceanographic context (T, S, $O_{2_{sat}}$)

A series of temperature and salinity maps (Figures 6a-d, A1, A2) illustrate the physical oceanographic properties of the Atlantic Zone. The Arctic waters of the Labrador Coastal Current on the northern NL Shelf are characterized by low salinities and temperatures near freezing, while the Scotian Slope surface is characterized by warmer (>18°C) and more saline (>33) Gulf Stream waters (Figure 2a). The lowest salinities (<27) are found in the surface waters of the LSLE (ignoring the Saguenay Fjord and the USLE; see Figure 3).

The moderately cold and saline surface waters along the southeastern NL Shelf and within the GSL consist of Arctic waters that have been modified by the Gulf Stream, St. Lawrence River, or warmed in summer. The freshwater exiting the LSLE can be traced at surface along the coast of the Gaspé peninsula into the southern GSL and Northumberland Strait (mean S~29), where it warms significantly in summer (mean summer T~16°C) (Figures A1, A2). The GSL encompasses the greatest sea surface temperature differences between spring and summer, yet the largest differences are from spring to fall and found on the Scotian Shelf (> 15°C). Since the AZMP does not include carbonate winter sampling, the coldest temperatures in this dataset, down to -1.7°C, are located within the CIL, in the subsurface waters of the NL Shelf (e.g., hydrographic section SI, Figure A10a) and in the GSL (e.g., hydrographic section LC, Figure A14a). Warm, saline bottom waters influenced by the Gulf Stream can be traced along the southwest Scotian Shelf and Laurentian Channel into the GSL. Shallow bottom waters of the GSL can warm in summer and exceed 17°C (not shown).

The oxygen saturation ($O_{2_{sat}}$, see methodology) is greatest at the surface with mean regional values > 90% and supersaturation occurring during spring plankton blooms (Figure 6e). Along the southern NL and Scotian outer shelf and slope, an oxygen minimum zone with $O_{2_{sat}}$ down to 45% is centered around 250 m (e.g. hydrographic section SESPB, Figure 9). Mean bottom values on the NL Shelf range from nearly 100% off Labrador to ~55% off southern NL. The $O_{2_{sat}}$ reaches supersaturation in the shallow bottom waters of the southern GSL and undersaturation in deeper areas associated with the Laurentian Channel. Hypoxia, which occurs at the bottom of the LSLE and deeper areas of the GSL such as the Laurentian, Anticosti and Esquiman Channels (Figure 1; see also Gilbert et al. (2005)), is shown as dark circles in Figure 6f.

Changes in the physical environment partially drives the variability in the carbonate system. In recent years, the proportion of Labrador Current Waters entering the deepest layers of the GSL in the Laurentian Channel has reduced at the expanse of an increase in the North Atlantic Central Waters (Jutras et al., 2020). This translated into a significant increase in the temperature

of the bottom layers of the GSL, together with a decrease in Dissolved Oxygen and pH (DFO, 2023). On the NL shelf, the variability of the cold and fresh Arctic-origin waters flowing southward along the coast influences the carbonate system, with more acidic conditions expected during the colder and fresher years (Cyr et al., 2022b). On the Scotian Shelf, warmer and saltier conditions usually imply that the system is less prone to the under saturation of the carbonate saturation states, but the changes in water masses composition may influence the interannual variability of carbonate parameters. In the next sub-section, we describe the carbonate system and make links, when possible, with the oceanography of the region.

4.2   Carbonate parameters (TA, DIC, pH, Ω_{arg})

This section comprises of a brief description of the spatial and temporal variations of carbonate parameters of the Atlantic Zone. Except for 2015, the values and seasonal cycles among annual surveys are relatively comparable. For this reason, we chose the year 2017, one of the most complete year to date, both seasonally and spatially. In the following, descriptions made of the Atlantic Zone thus refers to maps and sections from 2017 (Figures 6-8, A1-A9). Comparing seasonal changes (spring, summer, fall) of the Atlantic Zone or changes by region is difficult due to the surveying protocols established by each region. The hydrographic sections FC and BB on the NL Shelf (Figure 3a) are the only ones planned for the three seasons every year, however the station separation is greater along BB, and thus the resolution poorer. Although the standard AZMP GSL sections are only surveyed in spring and fall, the summer groundfish surveys between 2017 and 2022 provide enough data to evaluate some seasonal trends in the GSL (see below).

4.2.1   Total Alkalinity

The linear relationship between TA and S for the Atlantic Zone provides an $r^2 = 0.94$ ($TA = 40.34 \times S + 893.64, p < 0.001$; Figure 5), and consequently TA values follow the same spatial pattern as S (Figures $6c, d, 7a, b$, A2, A4). The lowest TA concentrations are located in surface waters of the LSLE and GSL due to freshwater outflow from the LSLE (TA value at S = 0 is $< 1200\,\mu\mathrm{mol\,kg}^{-1}$; see section Calculation of carbonate parameters), which are also observed exiting the GSL along southwest Cabot Strait onto the Scotian Shelf (Figure $7a$).

The surface TA is also low along the NL coast which is associated with coastal runoff and the fresh Labrador Coastal Current. Largest TA values, reaching nearly as high as $2400\,\mu\mathrm{mol\,kg}^{-1}$, are found within the upper 150 m of the southern NL and Scotian slope waters. Following the seasonal cycle of salinity, TA generally decreases from spring to summer/fall on the NL/Scotian Shelves, reflecting respectively the continued freshening of the NL coast (Cyr and Galbraith, 2021) and the freshwater export from the LSLE exiting the Gulf of St. Lawrence at Cabot Strait (Dever et al., 2016). Although the TA of the Atlantic Zone bottom waters follows a similar spatial pattern as the surface, the values are higher and the range is much narrower (Figure $7b$). The mean shelf bottom (< 600m) TA is $2241\,\mu\mathrm{mol\,kg}^{-1}$, with lowest values in the USLE and shallow southern GSL ($\sim 2000\,\mu\mathrm{mol\,kg}^{-1}$). The highest TA values of the Atlantic Zone are in the arm Slope Water ($\sim 2300\,\mu\mathrm{mol\,kg}^{-1}$) in deep waters of the Scotian Slope and GSL.

11

4.2.2 Dissolved Inorganic Carbon

The highest concentrations of DIC are located in the deepest areas (>275 m) of the LSLE and GSL specifically the Laurentian, Anticosti and Esquiman channels, with maximum values just over $2300\,\mu\mathrm{mol\,kg^{-1}}$(Figures 7$d$, A5). Moderately high concentrations are observed deep offshore along the NL (up to $2264\,\mu\mathrm{mol\,kg^{-1}}$) and Scotian (up to $2244\,\mu\mathrm{mol\,kg^{-1}}$) shelves and slopes. These values decrease on the shelf toward the coasts, and the lowest values are in the shallow areas of the shelf under freshwater influence (down to $\sim2000\,\mu\mathrm{mol\,kg^{-1}}$in the USLE). The accumulation of DIC within shelf bottom waters in fall is due to the remineralization of organic matter sinking to the bottom after spring and summer plankton blooms, with the highest values in the poorly ventilated deep GSL waters. The surface water has significantly lower DIC values, with the lowest concentrations occurring in the SLE, as well as the southern GSL and the coastal stations along the northern NL Shelf (Figure 7c).

In southern NL and the eastern GSL, the DIC decreases from spring to summer as it is consumed during the plankton bloom, then increases from summer to fall during the remineralization of that produced organic matter. The decrease in values from spring to fall along the Scotian Shelf reflects the transition from high winter DIC values due to remineralization, cold temperatures (increased solubility), and mixing with deep DIC enriched water during winter convection, to lower values in fall due to photosynthesis and stratification.

4.2.3 Partial pressure of CO_2

The lowest $p\mathrm{CO_2}$ values (down to $\sim200\,\mu\mathrm{atm}$) are located on the Newfoundland and Labrador Shelf, particularly in the coldest northern surface waters (Figures 7e, A6). $p\mathrm{CO_2}$ generally increase from surface to bottom and from spring to fall as plankton from the spring bloom is consumed (surface/spring) then remineralized (bottom/fall). Higher temperatures also influence the seasonal and southward increase in $p\mathrm{CO_2}$. Therefore, slightly higher values are located in the bottom waters of the southern NL and Scotian shelves and slopes, reaching a maximum ($\sim600\,\mu\mathrm{atm}$) at the O_2 minimum (Figure 9). Coincident with DIC, the highest $p\mathrm{CO_2}$ values are located in the deepest areas of the LSLE and GSL, with values $>1500\,\mu\mathrm{atm}$ (Figure A14). This CO_2, which accumulates at depth due to poor ventilation in the GSL, is produced by the remineralization of organic matter.

This study however highlights some sensitivity in the choice of the carbonate equilibria parameters used to derive $p\mathrm{CO_2}$ using CO2SYS (Table 2d). More precisely, results from the GSL (excluding the Saguenay) where TA, DIC and pH are measured (N=2150) suggest that using the pair TA/DIC would lead to a near 9% decrease in $p\mathrm{CO_2}$ estimate on average compared to using TA/pH or DIC/pH (with 95% of the variation within the [-27%, +2%] range). These results advocate for a direct measurement of $p\mathrm{CO_2}$ when possible and confirm the cautiousness needed with derived values (Golub et al., 2017).

4.2.4 pH

In 2017, the pH of the Atlantic Zone ranges from approximately 7.5 in the LSLE and GSL bottom waters (and lower in the Saguenay River) to 8.3 in the surface waters off Labrador, the highest values generally found along the shelf once the sea ice has melted in summer (Figures 8a-b, A7). The plankton bloom, which consumes CO_2, is concurrent with the ice retreat,

which increases the pH. Stations with high pH are often located away from shore with higher T, S and TA (Figure 6a-c, 8a), and less influenced by coastal processes. High pH is also observed during most annual spring surveys along the Scotian Shelf (particularly in 2017). These high pH values may be associated with the spring plankton bloom . The surface water pH is relatively uniform on the NL shelf (range [8.06, 8.10]) while it varies between 7.88 and 8.08 on the Scotian shelf and between 7.74 and 7.98 for the GSL. The decreased GSL surface pH is influenced by the freshwater exiting the LSLE (area of lowest surface pH) and high concentrations of plankton which consumes CO_2 (increases pH) and is subsequently remineralized (decreases pH).

The bottom waters of the GSL, specifically the LSLE and northern and deeper areas of the GSL including the Laurentian, Anticosti and Esquiman Channels, contain the lowest pH (down to 7.5 in 2017) of the Atlantic Zone (Figure 8b). These areas are also associated with the lowest $O_{2_{sat}}$ ($\sim$16% in 2017; Figure 6f). Due to the estuarine nature of the GSL, its bottom waters have restricted ventilation allowing for the accumulation of CO_2 and reduction in pH produced by the respiration of organic matter in this highly productive environment. The highest bottom pH values are located within the cold shallow bottom waters of the GSL and in the coldest waters of the NL Shelf. The bottom pH of the Atlantic Zone generally decreases throughout the year, likely due to the remineralization of organic matter (Figure A7). The spatial and temporal distribution of pH appears to be inversely correlated with pCO$_2$, which describes a pattern of the photosynthesis and subsequent remineralization of plankton.

Data from high-resolution Station Rimouski and Station 27 (Figure 4) show the spatial differences between the NL shelf and the GSL, as well as the interannual variability of pH in these regions. Station 27 exhibits higher pH in general with little difference between the surface and the bottom, although interannual variations are large. At Station Rimouski, a significant difference in pH exists between the surface and the bottom. There is also a documented significant decrease in pH in the bottom waters of the LSLE where Station Rimouski is located, reaching record low of 7.48 in October 2022 (Figure 4; top panel, orange line). This decrease in pH is accompanied with an increase of temperature at depth caused by the progression of warm waters in the deep channels of the GSL decrease and a decrease in dissolved oxygen saturation to unprecedented levels (<10%; not shown). Since 2018, these observations are reported as part of the AZMP annual reports (e.g., DFO, 2023).

4.2.5 Saturation state relative to Aragonite (Ω_{arg})

The Atlantic zone Ω_{arg} ranges from 0.5 in the LSLE and GSL bottom waters (lower values in the Saguenay River) to 3.7 in the surface waters of the southwest Scotian Slope (Figures 8c,d, A8). These highest Ω_{arg} surface waters are most influenced by the warm and saline Gulf Stream waters (Figure 6a, c and 8c, southernmost stations). $\Omega_{arg} > 2.0$ are also located in the surface waters of the outer NL shelf and slope. On average, these Scotian and NL waters increase in Ω_{arg} from spring to fall (Figure A8), corresponding to the seasonal temperature increase and decrease in S and TA (Figures A1, A2 and A4). Excluding the LSLE, the surface GSL Ω_{arg} values are similar to those from the southern NL and northeastern Scotian Shelves ($\sim$1.5 – 2.0). The surface waters of the USLE are undersaturated ($\Omega_{arg} < 1$) with respect to aragonite (and in some instances calcite) due to low TA and DIC (Figures A4, A5, A8 and A9), and can be traced into the GSL along the north coast of Gaspé. The bottom waters of the GSL, specifically the LSLE and northern and deeper areas of the GSL including the Laurentian, Anticosti and Esquiman channels, are undersaturated with respect to aragonite (Figure 8d).

Most of the bottom GSL samples (>90%) are undersaturated, with the few saturated samples in shallow areas or along the Cabot Strait section. The poorly ventilated GSL allows for the accumulation DIC produced by the decomposition of organic matter in this highly productive environment. The high DIC, coupled with a low buffering capacity (TA), produced the undersaturated benthic conditions. Undersaturated waters also occur on the southeast Scotian Shelf where GSL bottom water exits through Cabot Strait, as well as the southern (colder) NL Shelf. These conditions are present during summer (NL) and fall (MAR, NL) surveys due to the remineralization of the spring/summer plankton bloom. Although undersaturation is present, the mean Ω_{arg} on the NL and Scotian Shelves is ~1.3. The deep Scotian and NL Slopes are also undersaturated, and the saturation horizon ($\Omega_{arg}=1$) is between 2200 m and 2300 m (Figure 10). Azetsu-Scott et al. (2010) has demonstrated that in the Labrador Sea, this horizon corresponds to the depth where the Labrador Sea Water overlies the North East Atlantic Deep Water. Therefore, the depth of the saturation horizon along the Labrador Slope can fluctuate with time depending on the deep winter convection in the Labrador Sea (Azetsu-Scott et al., 2010; Yashayaev and Loder, 2017).

Similar to pCO_2, some variability exists between Ω parameters derived using CO2SYS with different carbonate equilibria pairs (Table 2d). In this case, using the pair TA/DIC would lead to about a 7% increase in Ω estimate on average compared to using TA/pH or DIC/pH (with 95% of the variation within the [-1%, 20%] range. While this variability is slightly less than for pCO_2, care must be taken in the interpretation of the results provided here.

4.3 General overview of physical and biogeochemical interactions

An overview of the Atlantic Zone oceanographic setting, as well as a description of the different carbonate parameters were provided in Sections 4.1 and 4.2, respectively. A large range of values and seasonal variations were found for the different parameters presented. These elements are now discussed together in a broader regional and seasonal context.

The surface of the Atlantic Zone is characterized by cold (Arctic) and warm (Atlantic) waters that undergo a seasonal warming and freshening. This seasonal freshening generally lowers TA and the capability of the system to buffer acidification. On the other hand, seasonal dynamics of phytoplankton blooms generally decrease inorganic carbon (e.g., DIC) in surface waters during the spring/summer as a result of photosynthesis. At depth, these values generally increase spring to fall as plankton from the spring bloom is degraded and inorganic material remineralized near the bottom.

The lowest pCO_2 values are located in the cold Coastal Labrador Current and the highest in the fresh waters of the LSLE. The lowest pH values are found in the GSL and the LSLE. This is especially true for the southern portion of the Gulf and in the deep (> 300m) layers of the Laurentian Channel. The most acidic waters of the Atlantic Zone are found in the Lower St. Lawrence Estuary, where pH has decreased by 0.2 to 0.3 between the 1930's and the early 2000's, a region affected by severe hypoxia (Mucci et al., 2011). These low and undersaturated conditions, which cover a large part of the Atlantic Zone, are concerning and not favourable for calcifying organisms.

Ω_{arg} increases at surface and in shallow areas of the shelf from spring to fall in most MAR and NL stations as a consequence of the seasonal temperature increase and decrease in S and TA coupled with high DIC of respired organic matter (see also Shadwick et al., 2011a, b, for a description of the CO_2 system seasonal cycle on the SS). Most of the bottom GSL is also undersaturated with respect to aragonite ($\Omega_{arg}<1$), except for a few saturated samples in shallow areas and along the Cabot

445 Strait section. Consistent with Azetsu-Scott et al. (2010), low Ω_{arg} are found in the cold and fresh (thus lower TA) Arctic-origin waters of the Coastal Labrador Current. These cold acidic waters are a prominent feature of the Atlantic Zone as they contribute to the LSW formation southwest of the Grand Banks. The LSW, which has a $\Omega_{arg} < 2$, partly forms the deep waters of the Laurentian Channel in the GSL (Gilbert et al., 2005) then continues southward on the Scotian Slope and along the Northeast US Coast. These low Ω_{arg} values can be traced to the deep Gulf of Maine. As the water temperature increases during their 450 journey towards the southern US, Ω_{arg} increases reaching $\sim$4.5 in the Gulf of Mexico (Wanninkhof et al., 2015).

This study demonstrates clear links between the physical environment and the carbonate system in the Atlantic Zone. Waters around Atlantic Canada have warmed over the last century as a consequence of anthropogenic climate change, and this trend is expected to continue in the future (Greenan et al., 2019). In this context, it is crucial to continue to monitor the physical and biogeochemical environment in the Atlantic Zone. While the 9 years time series presented here is relatively short, the 455 data presented generally support other studies suggesting that the rate of change in ocean acidification and de-oxygenation in Atlantic Canada may be greater than the global average (Claret et al., 2018; Bernier et al., 2018). The situation is especially dramatic in the GSL where the warm waters entering the deepest layers of the GSL significantly decreased Dissolved Oxygen and pH since about 2019 (Figure 4; see also DFO (2023)).

5 Conclusion

460 As a result of the increasing atmospheric CO_2 uptake, the ocean has undergone acidification during the 20th century and are projected to continue to acidify through the 21st century (Pörtner et al., 2019). Observation programs such as the AZMP are essential to monitor these changes and their consequences on ecosystems (e.g., Tilbrook et al., 2019). Because *in situ* observations are often scattered in time and space, ocean biogeochemical models are another important tool available to improve our understanding of seasonal, inter-annual and climatic variations of ocean acidification. As the field of biogeochemical modeling 465 is rapidly developing, the availability of biogeochemical data at meaningful spatial and temporal resolution however appears as a considerable challenge that hinders the implementation or validation of such models at regional scales (Fennel et al., 2019; Capotondi et al., 2019; Pilcher et al., 2019; Lavoie et al., 2021). In addition to providing a baseline of carbonate parameters, a comprehensive overview of carbonate parameters such as the one provided here is thus a necessary and useful contribution to the modeling community.

470 Using the decrease in Ω_{arg} of 0.5 ± 0.2 in the surface ocean by the year 2100 suggested by Bates et al. (2009), it appears that ocean acidification may impact parts of the ecosystem within the next century. As climate changes, however, the Atlantic Zone will be influenced by changes in temperature, salinity, ocean currents, nutrients and productivity, all of which will contribute to regional changes in pH and saturation state. While this study provides a useful baseline for the Atlantic Zone, incorporating these data into biogeochemical models is a necessary step in order to examine the regional response to ocean acidification and 475 the future of the Atlantic Canada aquaculture and fishing industries (Lavoie et al., 2020; Siedlecki et al., 2021).

6 Data availability

The full dataset of measured and derived parameters is available in the Federated Research Data Repository at https://doi.org/10.20383/102.0673 (Cyr et al., 2022a). It consists of a single comma-separated values (CSV) file named *AZMP_carbon.csv*. This file contains 17025 lines, each corresponding to a discrete sample. Out of this number, 15683 contains the full suite of parameters derived using *CO2sys*, the remaining 1342 samples have only one of the three carbonate parameters (TA, TIC or pH) available. A brief description of the columns in this file is provided here (see methods for a detailed description of the quantities):

- *Timestamp*: Date and Time (UTC) that the sample was collected in format 'yyyy-mm-dd HH:MM:SS'

- *Region*: Geographical region were the sample was collected ('GSL', 'MAR' or 'NL').

- *Trip_Name*: Name of the sea going mission (convention varies between regions).

- *Station_Name*: Hydrographic station names (e.g., 'TESL3', 'STN27', etc.).

- *Latitude_(degNorth)*: Latitude of the sampling in decimal format (in °N).

- *Longitude_(degEast)*: Longitude of the sampling in decimal format (in °E).

- *Depth_(dbar)*: Depth of the sampling (in decibars). In some rare circumstances, the nominal depth of the sample was used when the CTD depth was missing.

- *Temperature_(degC)*: Temperature (in °C) using the International Temperature Scale of 1990 (ITS-90)

- *Salinity_(psu)*: Salinity expressed on the practical salinity scale (psu, unitless)

- *Dissolved_Oxygen_(mL/L)*: Dissolved oxygen concentration (in $\mathrm{mL\,L^{-1}}$) obtained either by Winkler titration or DO sensor calibrated *in situ* with Winkler titration.

- *Nitrate_Concentration_(mmol/m3)*: Nitrate (and Nitrite) concentration (in $\mathrm{mmol\,m^{-3}}$) determined in laboratory with auto-analyzer.

- *Phosphate_Concentration_(mmol/m3)*: Phosphate concentration (in $\mathrm{mmol\,m^{-3}}$) determined in laboratory with auto-analyzer.

- *Silicate_Concentration_(mmol/m3)*: Silicate concentration (in $\mathrm{mmol\,m^{-3}}$) determined in laboratory with auto-analyzer.

- *Total_Alkalinity_(umol/kg)*: Total Alkalinity (TA in $\mathrm{\mu mol\,kg^{-1}}$), measured or derived using CO2SYS (no missing values).

- *Inorganic_Carbon_(umol/kg)*: Inorganic Carbon (DIC in $\mathrm{\mu mol\,kg^{-1}}$), measured or derived using CO2SYS (no missing values).

- *pH_tot_(total_scale)*: *in situ* pH on the total scale (unitless), derived using CO2SYS (no missing values).

505
- *Omega_Aragonite_(unitless)*: Saturation state relative to Aragonite (Ω_{arg}, unitless).

- *Omega_Calcite_(unitless)*: Saturation state relative to Calcite (Ω_{cal}, unitless).

- *pCO2_(uatm)*: Partial Pressure of CO_2 derived using CO2SYS (pCO_2, in μatmosphere).

- *Oxygen_Saturation_(%)*: Dissolved Oxygen Saturation (in %).

- *pH_lab_(total_scale)*: pH measured in the laboratory (total scale, unitless). The absence of value signifies that this
510   parameter was not measured.

- *pH_lab_temp_(degC)*: Temperature at which the pH was measured in the laboratory (in $^\circ$C).

- *Total_Alkalinity_Measured_(umol/kg)*: Total Alkalinity (TA in $\mu\mathrm{mol\,kg^{-1}}$) measured in the laboratory. The absence of value signifies that this parameter was not measured.

- *Inorganic_Carbon_measured_(umol/kg)*: Inorganic Carbon (DIC in $\mu\mathrm{mol\,kg^{-1}}$) measured in the laboratory. The absence
515   of value signifies that this parameter was not measured.

Note that the majority of the carbonate parameters data presented here have also been archived with extended metadata on the Ocean Carbon Data System (OCADS) accessible at the address https://www.ncei.noaa.gov/access/ocean-carbon-data-system/ (last access: 13 July, 2021). Users are invited to retrieve these data for more in depth analysis of the Atlantic zone carbonate system.

520   *Author contributions.* OG and FC led the study, writing, and the data processing and archiving. GM, KAS/CEG/SP, and MS provided the quality-controlled data for Newfoundland and Labrador shelf, the Scotian Shelf and the Gulf of St. Lawrence, respectively. PP, KAS and MS initiated the collection of carbonate parameters as part of the AZMP in 2014. All authors reviewed and commented the manuscript.

References

Azetsu-Scott, K., Clarke, A., Falkner, K., Hamilton, J., Jones, E. P., Lee, C., Petrie, B., Prinsenberg, S., Starr, M., and Yeats, P.: Calcium carbonate saturation states in the waters of the Canadian Arctic Archipelago and the Labrador Sea, Journal of Geophysical Research: Oceans, 115, 1–18, https://doi.org/10.1029/2009JC005917, 2010.

Azetsu-Scott, K., Starr, M., Mei, Z.-P., and Granskog, M.: Low calcium carbonate saturation state in an Arctic inland sea having large and varying fluvial inputs: The Hudson Bay system, Journal of Geophysical Research : Oceans, 119, 6210–6220, https://doi.org/10.1002/2014JC009948, 2014.

Bates, N. R., Mathis, J. T., and Cooper, L. W.: Ocean acidification and biologically induced seasonality of carbonate mineral saturation states in the western Arctic Ocean, Journal of Geophysical Research: Oceans, 114, 1–21, https://doi.org/10.1029/2008JC004862, 2009.

Belkin, I. M., Cornillon, P. C., and Sherman, K.: Fronts in Large Marine Ecosystems, Progress in Oceanography, 81, 223–236, https://doi.org/10.1016/j.pocean.2009.04.015, http://linkinghub.elsevier.com/retrieve/pii/S0079661109000330, 2009.

Bernier, R., Jamieson, R., Moore, A., and (eds.): State of the Atlantic Ocean Synthesis Report, Canadian Technical Report of Fisheries and Aquatic Sciences, 3167, iii + 149 p., https://waves-vagues.dfo-mpo.gc.ca/Library/40801755.pdf, 2018.

Brickman, D., Wang, Z., and DeTracey, B.: Variability of Current Streams in Atlantic Canadian Waters: A Model Study, Atmosphere - Ocean, 54, 218–229, https://doi.org/10.1080/07055900.2015.1094026, 2016.

Cai, W. J. and Wang, Y.: The chemistry, fluxes, and sources of carbon dioxide in the estuarine waters of the Satilla and Altamaha Rivers, Georgia, Limnology and Oceanography, 43, 657–668, https://doi.org/10.4319/lo.1998.43.4.0657, 1998.

Cai, W. J., Hu, X., Huang, W. J., Jiang, L. Q., Wang, Y., Peng, T. H., and Zhang, X.: Alkalinity distribution in the western North Atlantic Ocean margins, Journal of Geophysical Research: Oceans, 115, 1–15, https://doi.org/10.1029/2009JC005482, 2010.

Capotondi, A., Jacox, M., Bowler, C., Kavanaugh, M., Lehodey, P., Barrie, D., Brodie, S., Chaffron, S., Cheng, W., Dias, D. F., Eveillard, D., Guidi, L., Iudicone, D., Lovenduski, N. S., Nye, J. A., Ortiz, I., Pirhalla, D., Pozo Buil, M., Saba, V., Sheridan, S., Siedlecki, S., Subramanian, A., de Vargas, C., Di Lorenzo, E., Doney, S. C., Hermann, A. J., Joyce, T., Merrifield, M., Miller, A. J., Not, F., and Pesant, S.: Observational Needs Supporting Marine Ecosystems Modeling and Forecasting: From the Global Ocean to Regional and Coastal Systems, Frontiers in Marine Science, 6, https://doi.org/10.3389/fmars.2019.00623, 2019.

Chen, B., Cai, W.-J., and Chen, L.: The marine carbonate system of the Arctic Ocean: assessment of internal consistency and sampling considerations, summer 2010, Marine Chemistry, 176, 174–188, 2015.

Claret, M., Galbraith, E. D., Palter, J. B., Bianchi, D., Fennel, K., Gilbert, D., and Dunne, J. P.: Rapid coastal deoxygenation due to ocean circulation shift in the northwest Atlantic, Nature Climate Change, 8, 868, https://doi.org/10.1038/s41558-018-0263-1, http://dx.doi.org/10.1038/s41558-018-0263-1, 2018.

Clayton, T. D. and Byrne, R. H.: Spectrophotometric seawater pH measurements: total hydrogen ion concentration scale calibration of m-cresol purple and at-sea results, Deep Sea Research Part I: Oceanographic Research Papers, 40, 2115–2129, 1993.

Cooley, S. R. and Doney, S. C.: Anticipating ocean acidification's economic consequences for commercial fisheries, Environmental Research Letters, 4, https://doi.org/10.1088/1748-9326/4/2/024007, 2009.

Cyr, F. and Galbraith, P. S.: A climate index for the Newfoundland and Labrador shelf, Earth System Science Data, 13, 1807–1828, https://doi.org/10.5194/essd-13-1807-2021, 2021.

Cyr, F. and Larouche, P.: Thermal fronts atlas of Canadian coastal waters, Atmosphere-Ocean, 53, 212–236, https://doi.org/10.1080/07055900.2014.986710, 2015.

Cyr, F., Gibb, O., Azetsu-Scott, K., Chassé, J., Galbraith, P., Maillet, G., Pepin, P., Punshon, S., and Starr, M.: Ocean carbonate parameters on the Canadian Atlantic Continental Shelf, Federated Research Data Repository, https://doi.org/10.20383/102.0673, 2022a.

570 Cyr, F., Snook, S., Bishop, C., Galbraith, P. S., Chen, N., and Han, G.: Physical Oceanographic Conditions on the Newfoundland and Labrador Shelf during 2021, vol. 2022/040, http://www.dfo-mpo.gc.ca/csas-sccs/Publications/ResDocs-DocRech/2016/2016_079-eng.html, 2022b.

Dever, M., Hebert, D., Greenan, B. J., Sheng, J., and Smith, P. C.: Hydrography and Coastal Circulation along the Halifax Line and the Connections with the Gulf of St. Lawrence, Atmosphere - Ocean, 54, 199–217, https://doi.org/10.1080/07055900.2016.1189397, 2016.

DFO: Canada's Fisheries Fast Facts 2021, Fisheries and Oceans Canada, Ottawa, Canada, 2022.

575 DFO: Oceanographic conditions in the Atlantic zone in 2022, Sci. Advis. Sec. Sci. Advis. Rep., 2022/019, ISSN1919-5087, 2023.

Dickson, A. G.: Thermodynamics of the dissociation of boric acid in synthetic seawater from 273.15 to 318.15 K, Deep Sea Research Part A. Oceanographic Research Papers, 37, 755–766, 1990.

Dickson, A. G.: The carbon dioxide system in seawater: equilibrium chemistry and measurements, Guide to best practices for ocean acidification research and data reporting, 1, 17–40, 2010.

580 Dickson, A. G. and Millero, F. J.: A comparison of the equilibrium constants for the dissociation of carbonic acid in seawater media, Deep Sea Research Part A. Oceanographic Research Papers, 34, 1733–1743, 1987.

Dickson, A. G., Sabine, C. L., and Christian, J. R.: Guide to best practices for ocean CO2 measurements., North Pacific Marine Science Organization, 2007.

Dinauer, A. and Mucci, A.: Spatial variability in surface-water pCO 2 and gas exchange in the world's largest semi-enclosed estuarine system:

585 St. Lawrence Estuary (Canada)., Biogeosciences, 14, 2017.

Dinauer, A. and Mucci, A.: Distinguishing between physical and biological controls on the spatial variability of pCO2: A novel approach using OMP water mass analysis (St. Lawrence, Canada), Marine Chemistry, 204, 107–120, https://doi.org/10.1016/j.marchem.2018.03.007, https://doi.org/10.1016/j.marchem.2018.03.007, 2018.

Doney, S. C.: The growing human footprint on coastal and open-ocean biogeochemistry, Science, 328, 1512–1516, 2010.

590 Ekstrom, J. A., Suatoni, L., Cooley, S. R., Pendleton, L. H., Waldbusser, G. G., Cinner, J. E., Ritter, J., Langdon, C., Van Hooidonk, R., Gledhill, D., Wellman, K., Beck, M. W., Brander, L. M., Rittschof, D., Doherty, C., Edwards, P. E., and Portela, R.: Vulnerability and adaptation of US shellfisheries to ocean acidification, Nature Climate Change, 5, 207–214, https://doi.org/10.1038/nclimate2508, 2015.

Fabry, V. J., Seibel, B. A., Feely, R. A., and Orr, J. C.: Impacts of ocean acidification on marine fauna and ecosystem processes., ICES Journal of Marine Science, 64, 414–432, https://doi.org/10.2307/j.ctv8jnzw1.25, 2008.

595 Fassbender, A. J., Alin, S. R., Feely, R. A., Sutton, A. J., Newton, J. A., and Byrne, R. H.: Estimating Total Alkalinity in the Washington State Coastal Zone: Complexities and Surprising Utility for Ocean Acidification Research, Estuaries and Coasts, 40, 404–418, https://doi.org/10.1007/s12237-016-0168-z, http://dx.doi.org/10.1007/s12237-016-0168-z, 2017.

Fennel, K., Gehlen, M., Brasseur, P., Brown, C. W., Ciavatta, S., Cossarini, G., Crise, A., Edwards, C. A., Ford, D., Friedrichs, M. A., Gregoire, M., Jones, E., Kim, H. C., Lamouroux, J., Murtugudde, R., and Perruche, C.: Advancing marine biogeochemi-
600 cal and ecosystem reanalyses and forecasts as tools for monitoring and managing ecosystem health, Frontiers in Marine Science, 6, https://doi.org/10.3389/fmars.2019.00089, 2019.

Florindo-López, C., Bacon, S., Aksenov, Y., Chafik, L., Colbourne, E., and Penny Holliday, N.: Arctic ocean and hudson bay freshwater exports: New estimates from seven decades of hydrographic surveys on the Labrador shelf, Journal of Climate, 33, 8849–8868, https://doi.org/10.1175/JCLI-D-19-0083.1, 2020.

605 Galbraith, P. S.: Winter water masses in the Gulf of St. Lawrence, Journal of Geophysical Research, 111, https://doi.org/10.1029/2005JC003159, http://www.agu.org/pubs/crossref/2006/2005JC003159.shtml, 2006.

Gilbert, D., Sundby, B., Gobeil, C., Mucci, A., and Tremblay, G.-H.: A seventy-two-year record of diminishing deep-water oxygen in the St. Lawrence estuary: The northwest Atlantic connection, Limnology and Oceanography, 50, 1654–1666, https://doi.org/10.4319/lo.2005.50.5.1654, http://www.aslo.org/lo/toc/vol_50/issue_5/1654.html, 2005.

610 Golub, M., Desai, A. R., McKinley, G. A., Remucal, C. K., and Stanley, E. H.: Large Uncertainty in Estimating pCO2 From Carbonate Equilibria in Lakes, Journal of Geophysical Research: Biogeosciences, 122, 2909–2924, https://doi.org/10.1002/2017JG003794, 2017.

Greenan, B., James, T., Loder, J., P., P., Azetsu-Scott, K., Ianson, D., Hamme, R., Gilbert, D., Tremblay, J.-E., Wang, X., and Perrie, W.: Changes in Oceans Surrounding Canada, in: Canada's Changing Climate Report, edited by Bush, E. and Lemmen, D. S., vol. Chapter 7, p. p. 343–423, Government of Canada, Ottawa, ON, 2019.

615 Han, G., Lu, Z., Wang, Z., Helbig, J., Chen, N., and de Young, B.: Seasonal variability of the Labrador Current and shelf circulation off Newfoundland, Journal of Geophysical Research, 113, C10 013, https://doi.org/10.1029/2007JC004376, http://www.agu.org/pubs/crossref/2008/2007JC004376.shtml, 2008.

Humphreys, M. P., Gregor, L., Pierrot, D., van Heuven, S. M. A. C., Lewis, E. R., and Wallace, D. W. R.: PyCO2SYS: marine carbonate system calculations in Python, https://doi.org/10.5281/zenodo.3886559, https://doi.org/10.5281/zenodo.3886559, 2020.

620 Hunt, C. W., Salisbury, J. E., Vandemark, D., Aßmann, S., Fietzek, P., Melrose, C., Wanninkhof, R., and Azetsu-Scott, K.: Variability of USA East Coast surface total alkalinity distributions revealed by automated instrument measurements, Marine Chemistry, 232, https://doi.org/10.1016/j.marchem.2021.103960, 2021.

Johnson, K. M., Wills, K. D., Butler, D. B., Johnson, W. K., and Wong, C. S.: Coulometric total carbon dioxide analysis for marine studies: maximizing the performance of an automated gas extraction system and coulometric detector, Marine chemistry, 44, 167–187, 1993.

625 Jutras, M., Dufour, C. O., Mucci, A., Cyr, F., and Gilbert, D.: Temporal Changes in the Causes of the Observed Oxygen Decline in the St. Lawrence Estuary, Journal of Geophysical Research: Oceans, 125, https://doi.org/10.1029/2020JC016577, 2020.

Kroeker, K. J., Kordas, R. L., Crim, R., Hendriks, I. E., Ramajo, L., Singh, G. S., Duarte, C. M., and Gattuso, J. P.: Impacts of ocean acidification on marine organisms: Quantifying sensitivities and interaction with warming, Global Change Biology, 19, 1884–1896, https://doi.org/10.1111/gcb.12179, 2013.

630 Lavoie, D., Lambert, N., Rousseau, S., Dumas, J., Chassé, J., Long, Z., Perrie, W., Starr, M., Brickman, D., and Azetsu-Scott, K.: Projections of future physical and biogeochemical conditions in the Gulf of St . Lawrence , on the Scotian Shelf and in the Gulf of Maine, Can. Tech. Rep. Hydrogr. Ocean Sci., 334, xiii + 102 p., 2020.

Lavoie, D., Lambert, N., Starr, M., Chassé, J., Riche, O., Le Clainche, Y., Azetsu-Scott, K., Béjaoui, B., Christian, J. R., and Gilbert, D.: The Gulf of St. Lawrence Biogeochemical Model: A Modelling Tool for Fisheries and Ocean Management, Frontiers in Marine Science, 8, 635 1–29, https://doi.org/10.3389/fmars.2021.732269, 2021.

Lévy, M., Ferrari, R., Franks, P. J., Martin, A. P., and Rivière, P.: Bringing physics to life at the submesoscale, Geophysical Research Letters, 39, 1–13, https://doi.org/10.1029/2012GL052756, 2012.

Lewis, E. R. and Wallace, D. W. R.: CO2SYS-Program developed for the CO2 system calculations, in: Carbon Dioxide Inf Anal Center Report ORNL/CDIAC-105, 1998.

640 Loder, J. W., Petrie, B., and Gawarkiewicz, G.: The Coastal Ocean off Northeastern North America : A Large-Scale View, in: The Sea: Vol. 11, The Global Coastal Ocean: Regional Studies and Synthesis, edited by Robinson, A. and Brink, K. H., chap. 5, pp. 105–133, John Wiley and Sons, Inc., 1998.

Mathis, J. T., Cooley, S. R., Lucey, N., Colt, S., Ekstrom, J., Hurst, T., Hauri, C., Evans, W., Cross, J. N., and Feely, R. A.: Ocean acidification risk assessment for Alaska's fishery sector, Progress in Oceanography, 136, 71–91, 2015.

645   McDougall, T. J. and Barker, P. M.: Getting started with TEOS-10 and the Gibbs Seawater (GSW) Oceanographic Toolbox, May, SCOR/IAPSO WG127, 2011.

Mehrbach, C., Culberson, C. H., Hawley, J. E., and Pytkowicx, R. M.: Measurement of the apparent dissociation constants of carbonic acid in seawater at atmospheric pressure 1, Limnology and oceanography, 18, 897–907, 1973.

Millero, F. J.: The pH of estuarine waters, Limnology and Oceanography, 31, 839–847, 1986.

650   Millero, F. J.: Thermodynamics of the carbon dioxide system in the oceans, Geochimica et Cosmochimica Acta, 59, 661–677, 1995.

Millero, F. J.: The marine inorganic carbon cycle, Chemical Reviews, 107, 308–341, https://doi.org/10.1021/cr0503557, 2007.

Millero, F. J.: Carbonate constants for estuarine waters, Marine and Freshwater Research, 61, 139–142, 2010.

Mintrop, L., Pérez, F. F., González-Dávila, M., Santana-Casiano, M., and Körtzinger, A.: Alkalinity determination by potentiometry: Inter-calibration using three different methods, 2000.

655   Mitchell, M. R., Harrison, G., Pauley, K., Gagné, A., Maillet, G., and Strain, P.: Atlantic zonal monitoring program sampling protocol, Canadian Technical Report of Hydrography and Ocean Sciences, 223, iv+23 pp., 2002.

Mucci, A.: The solubility of calcite and aragonite in seawater at various salinities, temperatures, and one atmosphere total pressure, American Journal of Science, 283, 780–799, 1983.

Mucci, A., Starr, M., Gilbert, D., and Sundby, B.: Acidification of Lower St. Lawrence Estuary Bottom Waters, Atmosphere-Ocean, 49,
660   206–218, https://doi.org/10.1080/07055900.2011.599265, http://www.tandfonline.com/doi/abs/10.1080/07055900.2011.599265, 2011.

Mucci, A., Levasseur, M., Gratton, Y., Martias, C., Scarratt, M., Gilbert, D., Tremblay, J.-, Ferreyra, G., and Lansard, B.: Tidally-induced variations of pH at the head of the Laurentian Channel., Canadian Journal of Fisheries and Aquatic Sciences, pp. 2017–0007, https://doi.org/10.1139/cjfas-2017-0007, http://www.nrcresearchpress.com/doi/10.1139/cjfas-2017-0007, 2017.

Orr, J. C., Epitalon, J.-M., and Gattuso, J.-P.: Comparison of ten packages that compute ocean carbonate chemistry, Biogeosciences Discus-
665   sions, 12, 1483–1510, 2015.

Petrie, B. and Drinkwater, K.: Temperature and salinity variability on the Scotian Shelf and in the Gulf of Maine 1945-1990., Journal of Geophysical Research, 98, 20 079–20 089, 1993.

Pilcher, D. J., Naiman, D. M., Cross, J. N., Hermann, A. J., Siedlecki, S. A., Gibson, G. A., and Mathis, J. T.: Modeled effect of coastal biogeochemical processes, climate variability, and ocean acidification on aragonite saturation state in the bering sea, Frontiers in Marine
670   Science, 5, https://doi.org/10.3389/fmars.2018.00508, 2019.

Pörtner, H.-O., Roberts, D. C., Masson-Delmotte, V., Zhai, P., Tignor, M., Poloczanska, E., Mintenbeck, K., Nicolai, M., Okem, A., Petzold, J., and others: IPCC special report on the ocean and cryosphere in a changing climate, IPCC Intergovernmental Panel on Climate Change (IPCC), 2019.

Raimondi, L., Matthews, J. B. R., Atamanchuk, D., Azetsu-Scott, K., and Wallace, D. W. R.: The internal consistency of the marine carbon
675   dioxide system for high latitude shipboard and in situ monitoring, Marine Chemistry, 213, 49–70, 2019.

Shadwick, E. H., Thomas, H., Azetsu-Scott, K., Greenan, B. J., Head, E., and Horne, E.: Seasonal variability of dissolved inorganic carbon and surface water pCO2 in the Scotian Shelf region of the Northwestern Atlantic, Marine Chemistry, 124, 23–37, https://doi.org/10.1016/j.marchem.2010.11.004, http://dx.doi.org/10.1016/j.marchem.2010.11.004, 2011a.

Shadwick, E. H., Thomas, H., Azetsu-Scott, K., Greenan, B. J. W., Head, E., and Horne, E.: Seasonal variability of dissolved inorganic
680   carbon and surface water pCO2 in the Scotian Shelf region of the Northwestern Atlantic, Marine Chemistry, 124, 23–37, 2011b.

Siedlecki, S. A., Salisbury, J., Gledhill, D. K., Bastidas, C., Meseck, S., McGarry, K., Hunt, C. W., Alexander, M., Lavoie, D., Wang, Z. A., Scott, J., Brady, D. C., Mlsna, I., Azetsu-Scott, K., Liberti, C. M., Melrose, D. C., White, M. M., Pershing, A., Vandemark, D., Townsend, D. W., Chen, C., Mook, W., and Morrison, R.: Projecting ocean acidification impacts for the Gulf of Maine to 2050: new tools and expectations, Elementa: Science of the Anthropocene, 9(1), 62, https://doi.org/10.1525/elementa.2020.00062, 2021.

685 Therriault, J., Petrie, B., Pepin, P., Gagnon, J., Gregory, D., Helbig, J., Herman, A., Lefaivre, D., Mitchell, M., Pelchat, B., Runge, J., and Sameoto, D.: Proposal for a northwest zonal monitoring program, Canadian Technical Report of Hydrographic and Ocean Sciences, 194, vii + 57 p., 1998.

Thibodeau, B., Devernal, a., and Mucci, a.: Recent eutrophication and consequent hypoxia in the bottom waters of the Lower St. Lawrence Estuary: Micropaleontological and geochemical evidence, Marine Geology, 231, 37–50, https://doi.org/10.1016/j.margeo.2006.05.010,
690 http://linkinghub.elsevier.com/retrieve/pii/S0025322706001277, 2006.

Tilbrook, B., Jewett, E. B., DeGrandpre, M. D., Hernandez-Ayon, J. M., Feely, R. A., Gledhill, D. K., Hansson, L., Isensee, K., Kurz, M. L., Newton, J. A., Siedlecki, S. A., Chai, F., Dupont, S., Graco, M., Calvo, E., Greeley, D., Kapsenberg, L., Lebrec, M., Pelejero, C., Schoo, K. L., and Telszewski, M.: An enhanced ocean acidification observing network: From people to technology to data synthesis and information exchange, Frontiers in Marine Science, 6, https://doi.org/10.3389/fmars.2019.00337, 2019.

695 Uppstrom, L. R.: The boron/chlorinity ratio of deep-sea water from the Pacific Ocean, Deep Sea Research, 21, 161–162, 1974.

Waldbusser, G. G., Hales, B., Langdon, C. J., Haley, B. A., Schrader, P., Brunner, E. L., Gray, M. W., Miller, C. A., and Gimenez, I.: Saturation-state sensitivity of marine bivalve larvae to ocean acidification, Nature Climate Change, 5, 273–280, https://doi.org/10.1038/nclimate2479, 2015.

Wanninkhof, R., Barbero, L., Byrne, R., Cai, W.-J., Huang, W.-J., Zhang, J.-Z., Baringer, M., and Langdon, C.: Ocean acidification along the
700 Gulf Coast and East Coast of the USA, Continental Shelf Research, 98, 54–71, 2015.

Wilson, T. J., Cooley, S. R., Tai, T. C., Cheung, W. W., and Tyedmers, P. H.: Potential socioeconomic impacts from ocean acidification and climate change effects on Atlantic Canadian fisheries, PLoS ONE, 15, 1–29, https://doi.org/10.1371/journal.pone.0226544, 2020.

Yashayaev, I. and Loder, J. W.: Further intensification of deep convection in the Labrador Sea in 2016, Geophysical Research Letters, 44, 1429–1438, https://doi.org/10.1002/2016GL071668, 2017.

Table 1. Summary of all surveys conducted in the Atlantic Zone that collected carbonate chemistry data from fall 2014 to 2022 that are included in this dataset. Note that the number of bottle correspond to the sample that include at least one of the carbonate parameters (TA, DIC or pH and might not signify that the full suite of parameters derived using CO2sys). Targeted measured parameters for each mission are provided in the last column.

Year	Season	Region	Trip Name	Stations	Bottles	Max Depth	Start Date	End Date	Measured Param.
2014	spring	GSL	M14010	1	43	330	2014-04-25	2014-12-16	TA, pH
	fall	GSL	IML201437	57	316	465	2014-10-27	2014-11-09	TA, DIC, pH
		MAR	18HU14030	37	241	2905	2014-09-19	2014-10-08	TA, DIC, pH
		NL	HUD114	37	254	1071	2014-11-16	2014-12-07	TA, DIC, pH
2015	spring	GSL	IML2015010	1	174	331	2015-01-18	2015-12-18	TA, pH
		GSL	IML201516	9	51	452	2015-06-01	2015-06-12	pH
		MAR	18HU15004	21	142	2941	2015-04-18	2015-04-25	TA, DIC
		NL	TEL144	26	137	533	2015-04-12	2015-04-27	TA, DIC
	summer	NL	TEL148	43	255	1009	2015-07-09	2015-07-26	TA, DIC
	fall	GSL	IML2015041	14	85	464	2015-10-19	2015-11-05	TA, pH
		MAR	18HU15030	51	386	5044	2015-09-20	2015-10-08	TA, DIC
		NL	HUD115	43	254	3676	2015-11-15	2015-12-06	TA, DIC
2016	spring	GSL	IML2016010	1	201	333	2016-01-23	2016-12-12	TA, pH
		GSL	IML2016015	19	110	459	2016-06-01	2016-06-26	TA, pH
		MAR	18HU16003	15	106	1254	2016-04-10	2016-04-25	TA, DIC
		MAR	18HU16006	15	191	4717	2016-05-02	2016-05-24	TA, DIC
		NL	TEL157	7	32	446	2016-04-01	2016-04-06	TA, DIC
		NL	TEL159	15	104	1210	2016-05-11	2016-05-17	TA, DIC
	summer	NL	TEL160	32	215	1074	2016-07-08	2016-07-28	TA, DIC
	fall	GSL	IML2016050	55	202	465	2016-10-16	2016-11-02	TA, pH
		MAR	18HU16027	60	377	3947	2016-09-16	2016-10-04	TA, DIC
		NL	HUD116	23	145	3303	2016-11-13	2016-11-20	TA, DIC

Table 1. [continued]

Year	Season	Region	Trip Name	Stations	Bottles	Max Depth	Start Date	End Date	Measured Param.
2017	spring	GSL	IML2017050	1	170	333	2017-02-07	2017-12-04	TA, pH
			IML2017080	40	224	466	2017-05-30	2017-06-19	TA, pH
			PER2017016	6	18	65	2017-06-15	2017-06-16	TA, pH
			PER2017018	4	8	20	2017-06-23	2017-06-28	TA, pH
		MAR	18OL17001	46	265	3000	2017-04-19	2017-05-01	TA, DIC
		NL	TEL173	51	363	1208	2017-04-06	2017-04-23	TA, DIC
	summer	GSL	PER2017024	40	80	49	2017-07-12	2017-07-30	TA, pH
			IML2017027	28	148	524	2017-08-03	2017-09-01	TA, pH
			PER2017026	27	81	136	2017-08-16	2017-08-21	TA, pH
			MLB2017001B	9	30	454	2017-08-25	2017-08-30	TA, pH
		NL	TEL176	48	352	1252	2017-07-08	2017-07-28	TA, DIC
	fall	GSL	IML2017048	46	223	455	2017-11-04	2017-11-23	TA, pH
		MAR	32EV17606	56	324	3757	2017-11-24	2017-12-15	TA, DIC
		NL	DIS009	27	195	1201	2017-11-11	2017-12-16	TA, DIC
2018	spring	GSL	IML2018040	1	364	331	2018-03-12	2018-12-06	TA, pH
			IML2018014	70	275	458	2018-06-05	2018-06-24	TA, pH
		MAR	18HU18004	43	320	4513	2018-04-08	2018-04-23	TA, DIC
		NL	TEL185	33	213	1200	2018-04-06	2018-04-24	TA, DIC
	summer	GSL	PER2018041	40	80	45	2018-07-11	2018-07-30	TA, pH
			IML201841	36	156	483	2018-08-03	2018-08-31	TA, pH
			PER2018042	32	96	136	2018-08-13	2018-08-21	TA, pH
		NL	COR011	80	492	1202	2018-07-15	2018-08-02	TA, DIC
	fall	GSL	TEL2018196	36	120	388	2018-09-07	2018-10-01	TA, pH
			PER2018043	6	14	89	2018-09-27	2018-10-07	TA, pH
			IML2018028	31	154	459	2018-10-23	2018-11-01	TA, pH
		MAR	18HU18030	49	361	4144	2018-09-15	2018-10-05	TA, DIC
		NL	HUD118	46	318	3677	2018-11-11	2018-12-02	TA, DIC

Table 1. [continued]

Year	Season	Region	Trip Name	Stations	Bottles	Max Depth	Start Date	End Date	Measured Param.
2019	spring	GSL	IML2019040	1	188	332	2019-04-12	2019-12-13	TA, pH
			IML201909	71	276	460	2019-05-26	2019-06-15	TA, pH
		MAR	COR2019001	42	295	3770	2019-04-09	2019-04-25	TA, DIC
		NL	TEL197	15	105	1197	2019-04-12	2019-04-18	TA, DIC
			TEL199	1	7	100	2019-04-20	2019-04-20	DIC
			TEL200	55	432	1207	2019-06-27	2019-07-13	TA, DIC
	summer	GSL	PER2019140	30	60	46	2019-07-23	2019-08-05	TA, pH
			IML2019036	20	101	516	2019-08-15	2019-09-03	TA, pH
			PER2019008	20	60	134	2019-08-15	2019-08-18	TA, pH
	fall	GSL	TEL2019201	35	126	372	2019-09-09	2019-10-01	TA, DIC, pH
			PER2020019	5	14	89	2019-09-22	2019-10-07	TA, DIC, pH
			IML2019049	45	228	470	2019-10-22	2019-11-06	TA, DIC, pH
		NL	COO001	43	306	1220	2019-11-17	2019-12-10	TA, DIC
2020	spring	GSL	IML2020040	1	120	332	2020-01-06	2020-12-09	TA, DIC, pH
	summer	NL	TEL210	43	313	1209	2020-07-14	2020-07-31	TA, DIC
			AMU014	1	5	150	2020-08-11	2020-08-11	TA, DIC
	fall	GSL	IML2020028	39	206	470	2020-10-19	2020-10-30	TA, DIC, pH
		MAR	HUD2020063	34	255	2000	2020-10-04	2020-10-14	TA, DIC
		NL	HUD120	36	261	3668	2020-11-10	2020-12-01	TA, DIC

Table 1. [continued]

Year	Season	Region	Trip Name	Stations	Bottles	Max Depth	Start Date	End Date	Measured Param.
2021	spring	GSL	IML2021011	1	150	332	2021-04-08	2021-12-16	TA, pH
		GSL	IML2021012	41	218	466	2021-06-02	2021-06-12	TA, pH
			IML2021014	30	59	397	2021-06-12	2021-06-22	TA, pH
		NL	TEL220	51	355	1204	2021-06-29	2021-07-19	TA, DIC
	summer	GSL	PER2021151	35	70	58	2021-07-06	2021-08-02	TA, pH
			IML2021030	31	153	529	2021-07-27	2021-08-24	TA, pH
			PER2021156	17	49	113	2021-08-30	2021-09-08	TA, pH
			CJC2021222	36	104	352	2021-08-31	2021-09-26	TA, pH
			PER2021021	2	6	92	2021-09-25	2021-09-25	TA, pH
	fall	GSL	IML2021044	50	307	469	2021-10-12	2021-10-26	TA, pH
		MAR	HUD2021185	63	409	4712	2021-09-17	2021-10-01	TA, DIC
		NL	TEL228	1	6	150	2021-12-20	2021-12-20	TA, DIC
2022	spring	GSL	IML202201	1	120	334	2022-04-27	2022-12-07	TA, DIC, pH
			IML2022021	74	325	468	2022-06-06	2022-06-26	TA, DIC, pH
			PER2022152	36	72	43	2022-06-30	2022-08-02	TA, DIC, pH
		MAR	AT4802	59	332	3775	2022-03-22	2022-04-04	TA, DIC
		NL	TEL229	1	6	150	2022-01-10	2022-01-10	TA, DIC
			TEL227	1	6	150	2022-01-20	2022-01-20	TA, DIC
			ATL001	57	427	4292	2022-04-10	2022-05-01	TA, DIC
	summer	GSL	IML2022039	25	157	521	2022-08-12	2022-09-14	TA, DIC, pH
			PER202223330	2	6	96	2022-09-08	2022-09-08	TA, DIC, pH
			CAR2022025	32	118	276	2022-09-13	2022-09-30	TA, DIC, pH
			PER2022022	7	19	91	2022-09-28	2022-09-30	TA, DIC, pH
		NL	NED558	2	12	150	2022-07-01	2022-07-02	TA, DIC
			PER004	1	6	150	2022-08-18	2022-08-18	TA, DIC
	fall	GSL	IML2022054	51	321	467	2022-10-25	2022-11-08	TA, DIC, pH
		NL	COO002	38	290	3676	2022-10-22	2022-11-08	TA, DIC

Table 2. Variability in calculated carbonate parameters using CO2SYS due to different sets of variables: a) Variability due to the choice of dissociation constants for low salinities (Mehrbach et al. (1973) as refit by Dickson and Millero (1987) (Mdm) rather than Cai and Wang (1998)). b) Variability due to the presence/absence of nutrients for the two sets of input pairs. c) Sensitivity of the calculated TA from linear relationship with salinity (determined by multiplying the linear fit by twice its standard deviation). The absence of pH data at salinities < 20 is due to the fact that these low salinities are located in the GSL which is the region that measures pH. d) Variability of the calculated carbonate parameters using CO2SYS with different carbonate equilibria pairs when all thre parameters are available. We used data for the GSL region only where most of these data occur.

Difference (%)	pH	Ω_{arg}	Ω_{cal}	$p\mathrm{CO}_2$	DIC	TA
a) Choice of dissociation constant						
$S_A < 20$	0.2	0.8	0.8	4	0.2	0
$S_A \geq 20$	-0.006	0.8	0.8	-0.5	-0.02	<0.001
b) Using nutrients in CO2sys						
TA/DIC (nutrients - no nutrients)	-0.03	-0.5	-0.5	-0.5	0	0
TA/pH (nutrients - no nutrients)	0.003	0.05	0.05	-0.05	0	0.08
c) Error when inferring TA from S_A (Spring 2015, GSL; N=493)						
TA/pH ($\pm 2\sigma$ on predicted TA)	0	± 0.03	± 0.03	± 0.03	± 0.03	± 0.03
d) Variability carbonate equilibria pairs (GSL only, S>20; N=2150)						
TA/DIC vs TA/pH	0.4	7	7	-9	-0.5	N/A
TA/DIC vs DIC/pH	0.4	7	7	-9	N/A	0.5
DIC/pH vs TA/pH	<0.001	-0.5	-0.5	-0.6	-0.5	-0.5
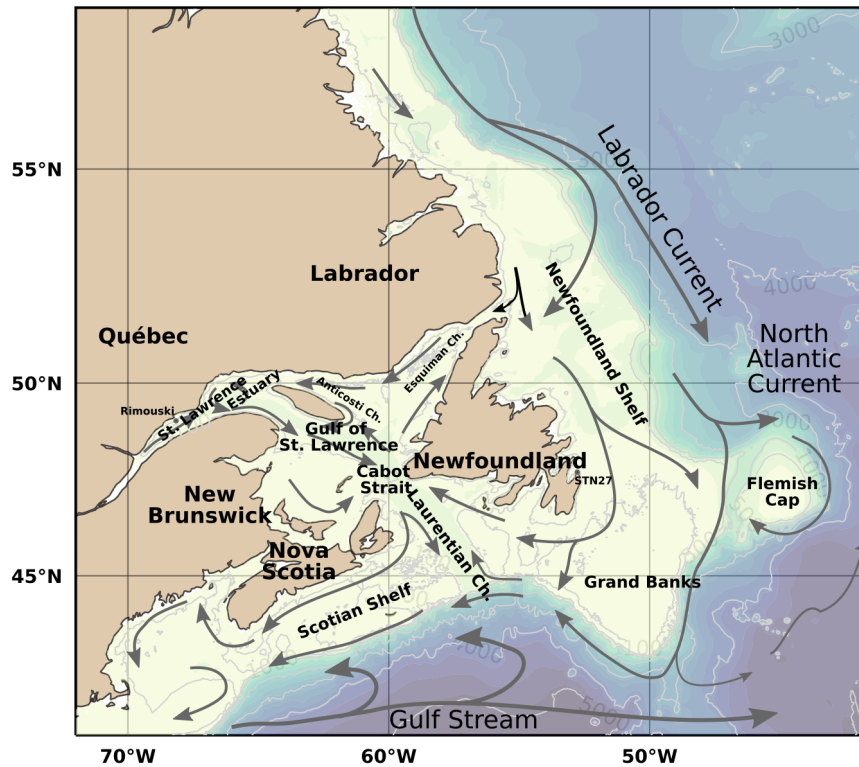
Figure 1. Bathymetric map of the Northwest Atlantic which includes the Newfoundland and Labrador Shelves and Slopes, Scotian Shelf and Slope, Gulf of St. Lawrence, and the St. Lawrence Estuary as the Atlantic Zone. Also identified are the deep channels within the Gulf of St. Lawrence: the Laurentian, Anticosti and Esquiman Channels. The approximate position and direction of the major current systems and their shelf and slope components are illustrated as arrows: Gulf Stream (gray) and Labrador Current (black).
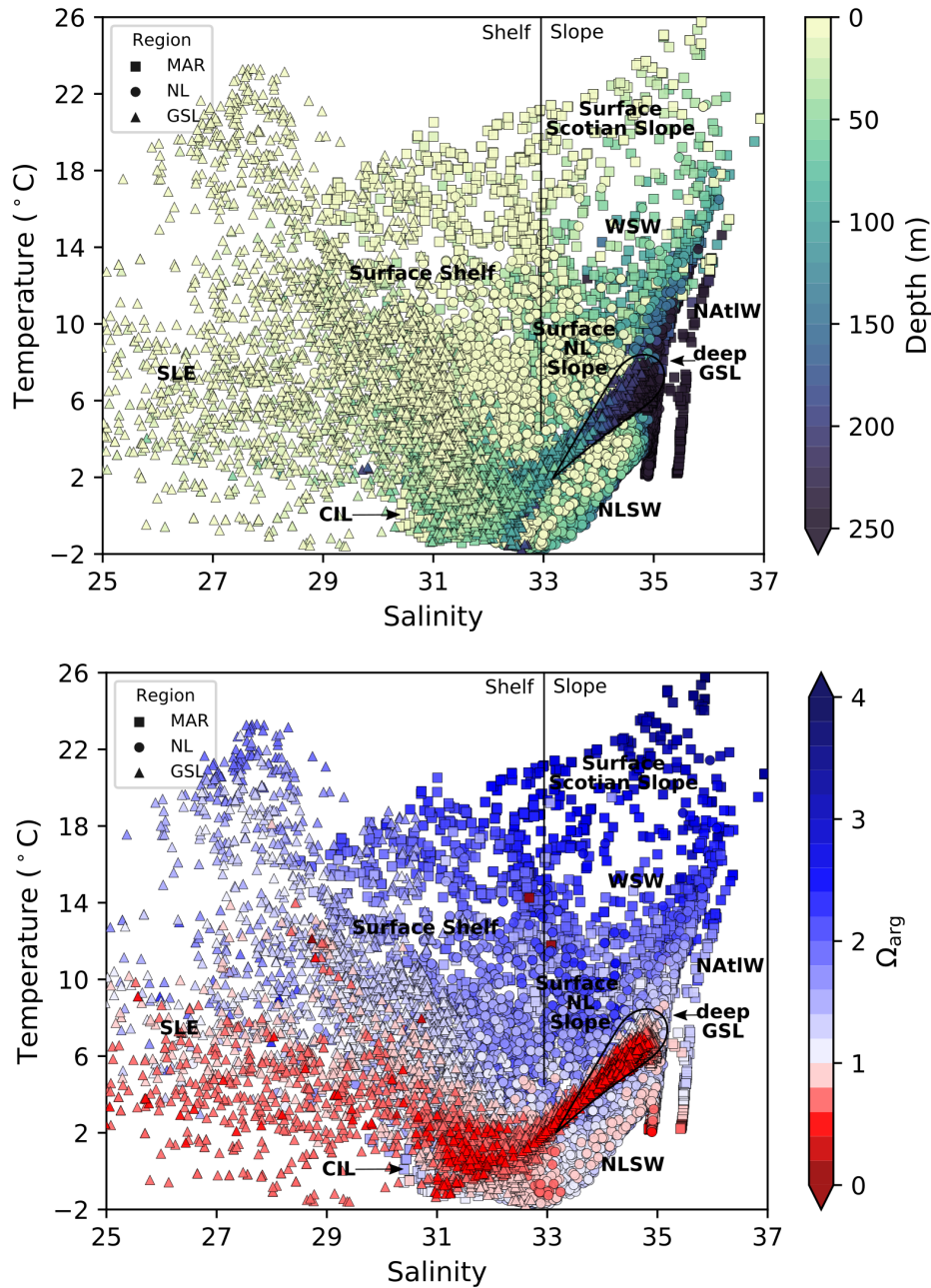
Figure 2. Diagrams of temperature - salinity versus depth (left) and temperature - salinity versus saturation state relative to aragonite for all bottle samples in the dataset. The three Regions of the Atlantic Zone are shown with different markers. An approximate division between the shelf and slope surface waters is indicated by the vertical black line at salinity 33. Various water masses are labeled (WSW = Warm Slope Water, NAtlW = North Atlantic Water, NLSW = Newfoundland and Labrador Slope Water). In the absence of clear water mass definition, the origin of the water is labeled (LSLE = Lower St. Lawrence Estuary, GSL = Gulf of St. Lawrence, LS = Labrador Shelf).
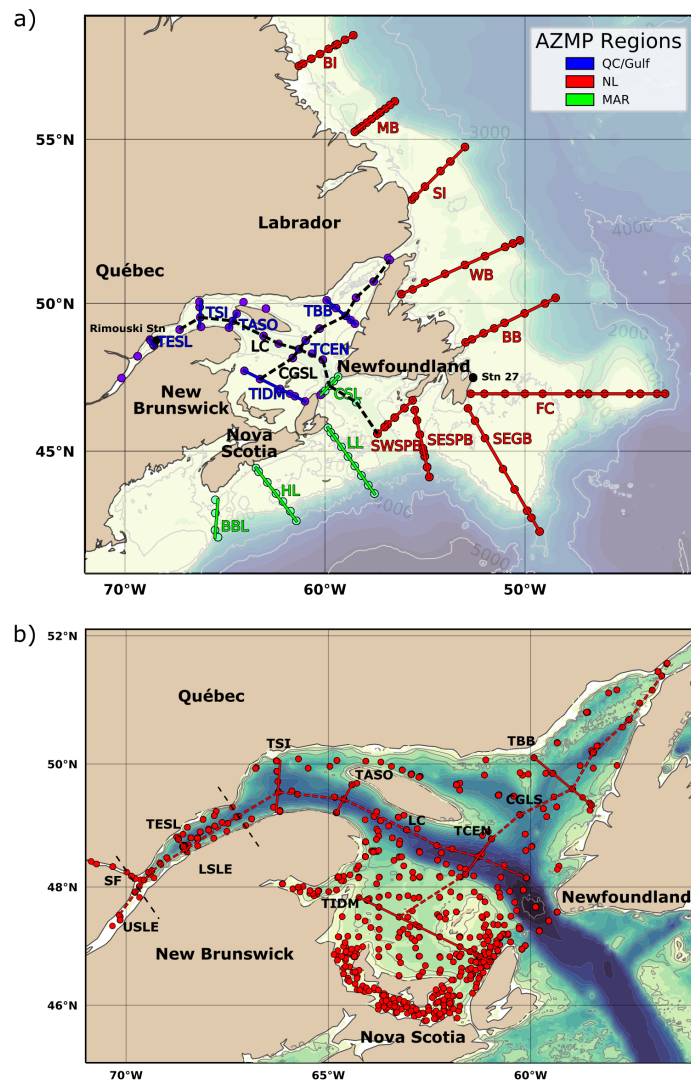
Figure 3. Bathymetric maps of the Atlantic Zone. AZMP surveys of the four Regions which include Maritimes (MAR), Newfoundland and Labrador (NL), and Québec (QC) and Gulf which have been combined as the Gulf of St. Lawrence (GSL) Region. The map of the Atlantic Zone in panel *a* shows the locations of the standard AZMP sections (from north to south and in the GSL): *Beachy Island* (BI), *Makkovik Bank* (MB), *Seal Island* (SI), *White Bay* (WB), *Bonavista Bay* (BB), *Flemish Cap* (FC), *Southeast Grand Bank* (SEGB), *Southeast St. Pierre Bank* (SESPB), *Southwest St. Pierre Bank* (SWSPB), *Cabot Strait Line* (CSL), *Louisbourg Line* (LL), *Halifax Line* (HL), *Browns Bank Line* (BBL), *Transect Bonne Bay* (TBB), *Transect Central* (TCEN), *Transect Iles de la Madeleine* (TIDM), *Transect Anticosti South* (TASO), *Transect Sept-Iles* (TSI), *Transect Estuaire du Saint-Laurent* (TESL) and *Laurentian Channel* (LC) from west to east across the entire GSL (e.g., Fig. A14). Panel *b* zooms in on the GSL Region and includes other sampling locations from in the dataset, such as the summer groundfish surveys. Here the Lower St. Lawrence Estuary (LSLE) correspond to the upstream portion of the GSL. The Upper St. Lawrence Estuary (USLE) and the Saguenay Fjord (SF) are also annotated.
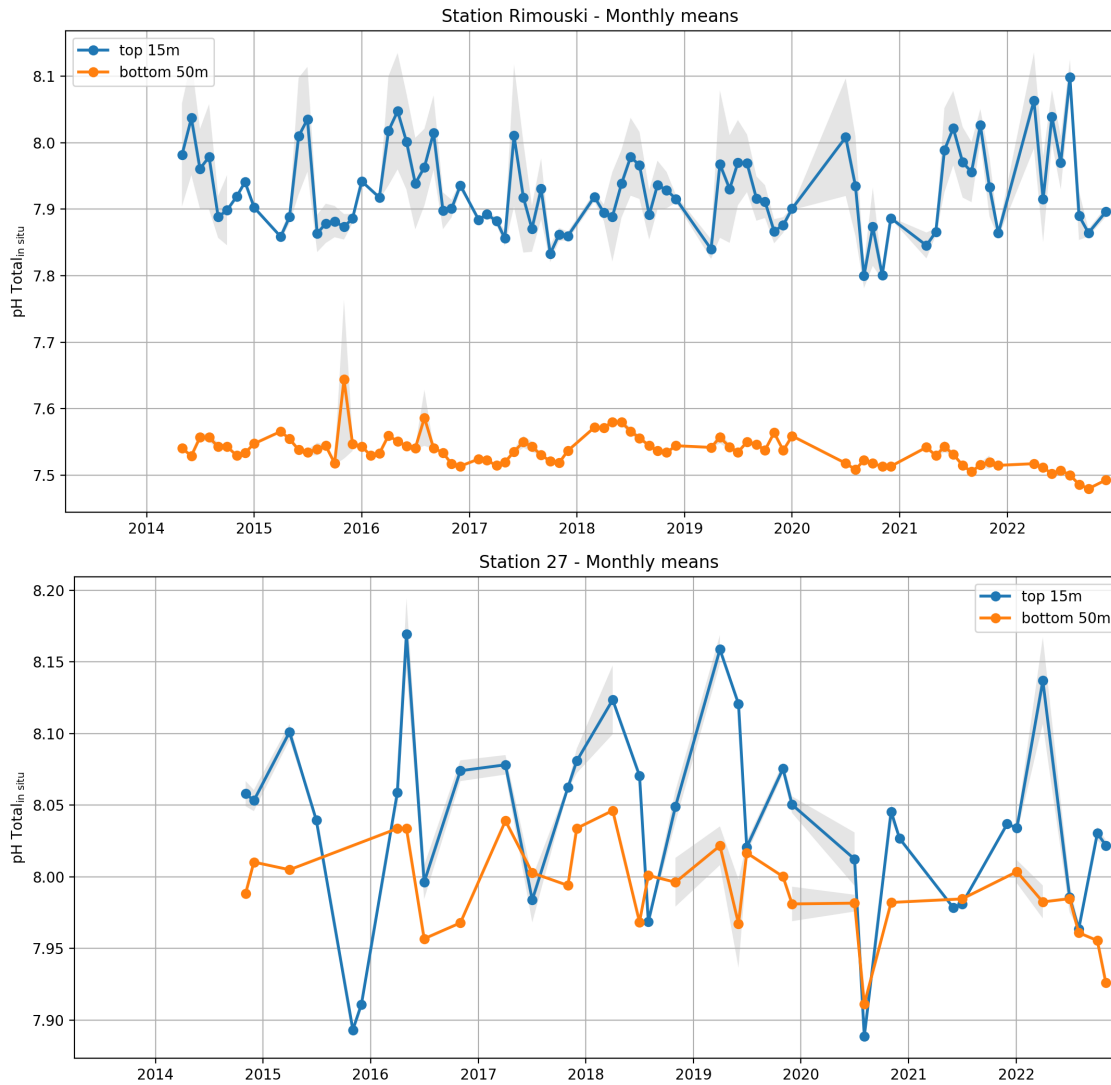
Figure 4. Monthly averages of pH data at Station Rimouski (top) and Station 27 (bottom). Surface observations (blue curves) are considered the average of the top 15m and bottom observations (orange curves) are the average of the bottom 50m. The shaded area correspond to ±0.5 SD of the monthly distribution (when more than one visit per month is made). The tick marks on the horizontal axis correspond to the beginning of the year.
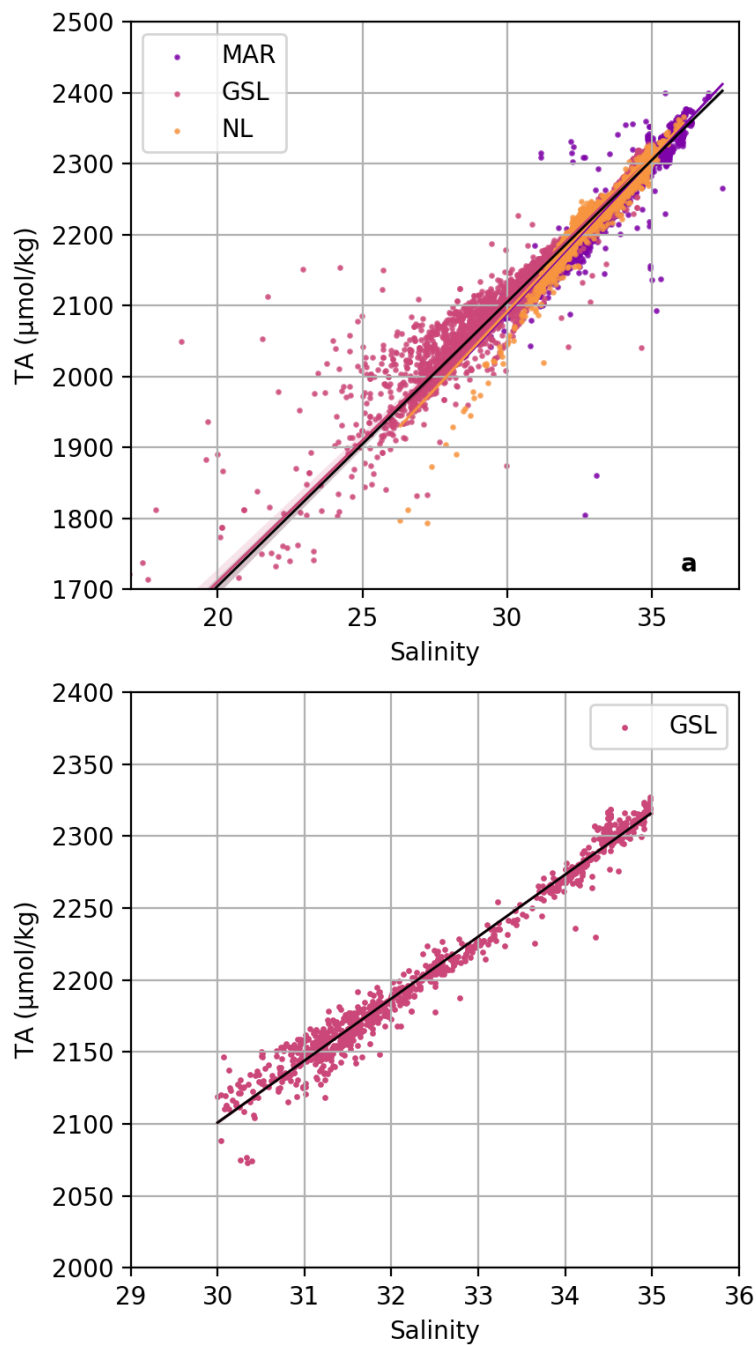
Figure 5. Scatter plot of total alkalinity (TA; μmol/kg) versus salinity. a) all samples (2014 – 2020) are A linear fit between TA and salinity have been established independently established for each region (colored lines according to the legend) and for the entire dataset (black line). The latter TA and salinity relationship is TA = 40.05 x S + 872.05, r2 = 0.94, p < 0.001. b) A linear relationship is also established for the GSL spring data with $S \geq 30$ only. This relationship between TA and salinity (TA = 43.09 x S + 808.31, r2 = 0.98, p < 0.001) is used in Section 3.3 to correct for missing TA data.
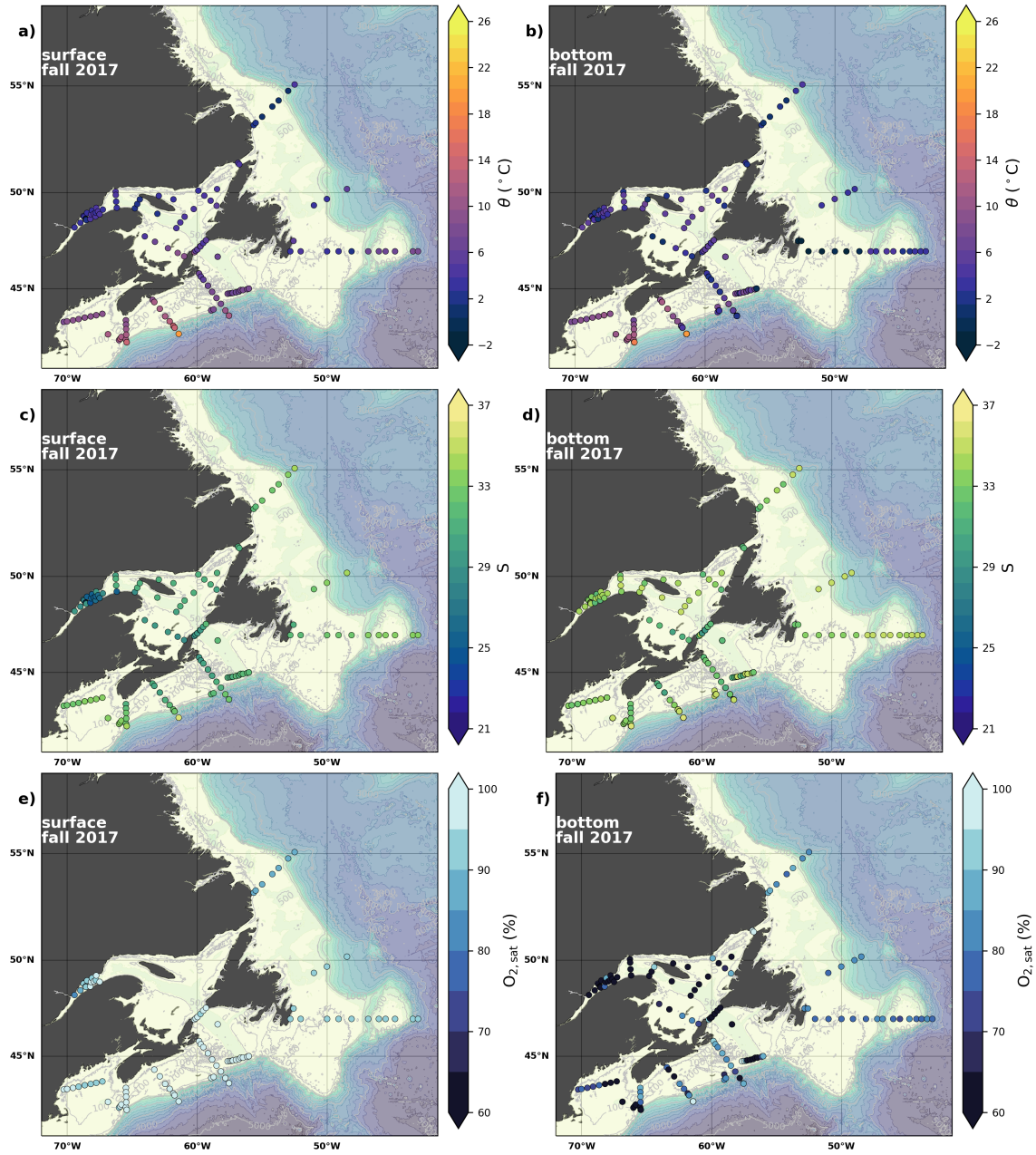
Figure 6. Maps of surface (upper most sample <52m; left side) and bottom (deepest sample >50m; right side) temperature (a, b), salinity (c, d) and oxygen saturation ($O_{2_{sat}}$) (e, f) for fall 2017. The GSL surface $O_{2_{sat}}$ is represented by samples at 50 m.
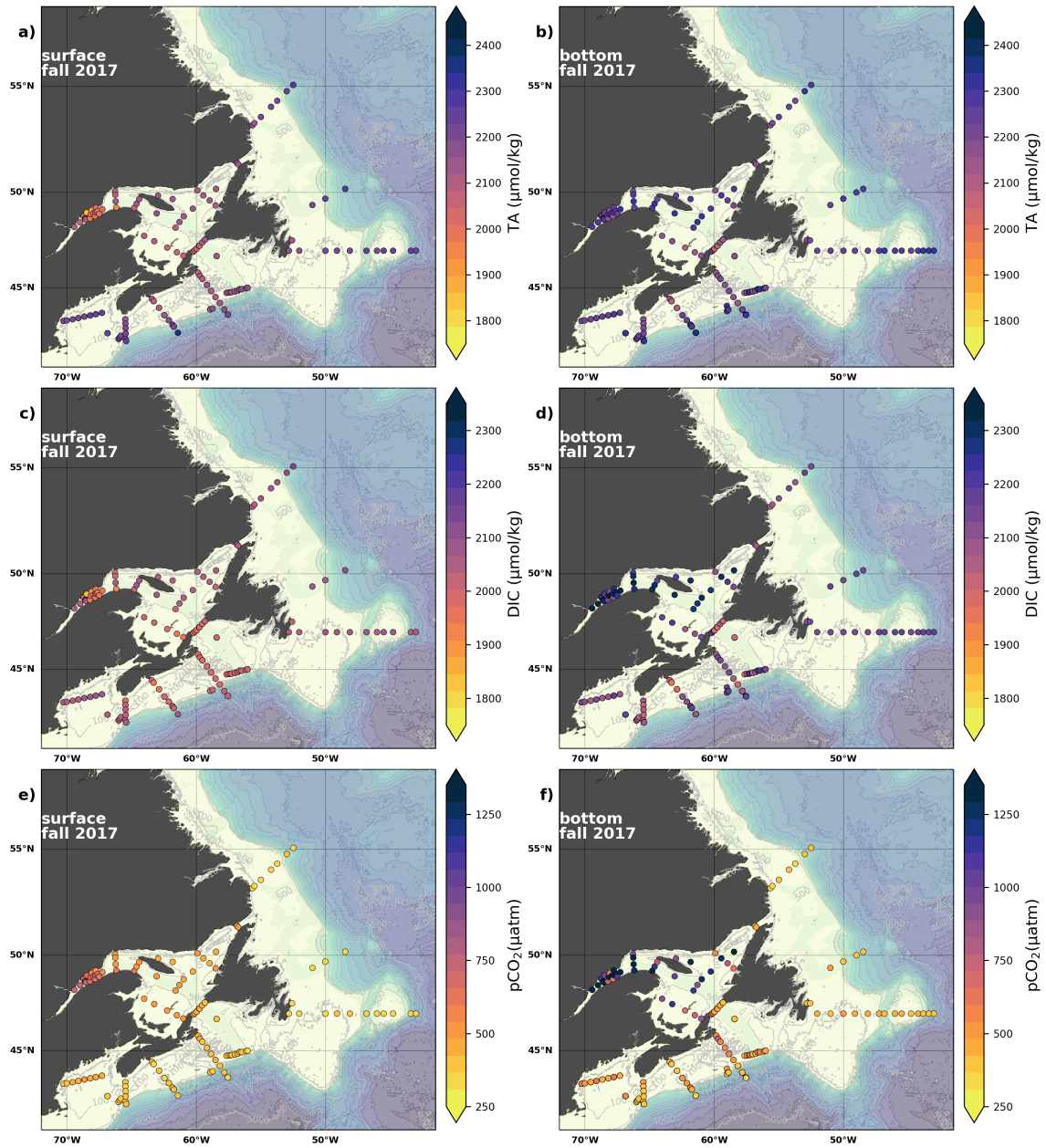
Figure 7. Maps of surface (upper most sample <52m; left side) and bottom (deepest sample <50m; right side) TA (a, b), DIC (c, d) and pCO$_2$ (e, f) for fall 2017.
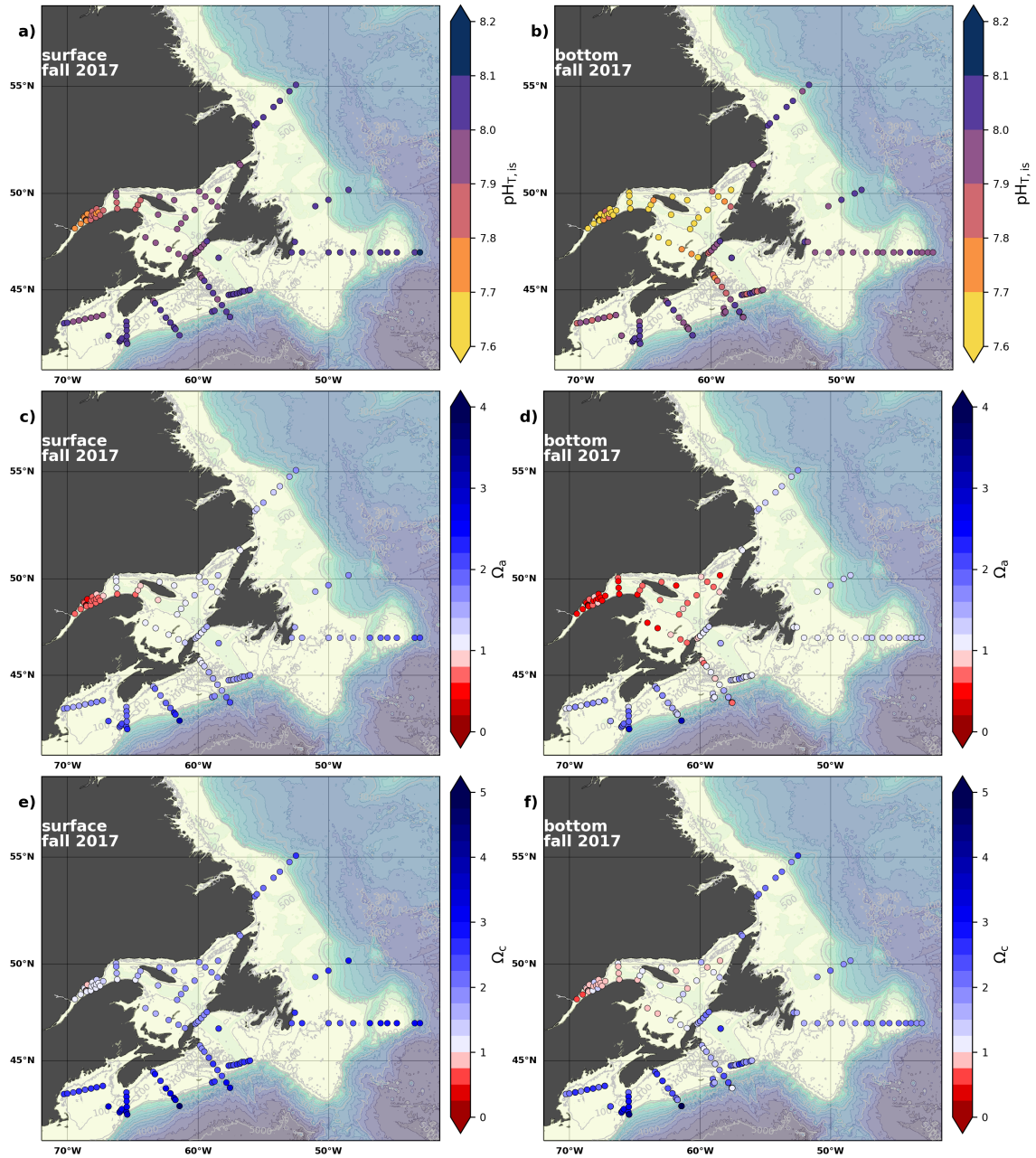
Figure 8. Maps of surface (upper most sample <52m; left side) and bottom (deepest sample >50m; right side) pH (a, b), Ωarg (c, d) and Ωcal (e, f) for fall 2017.
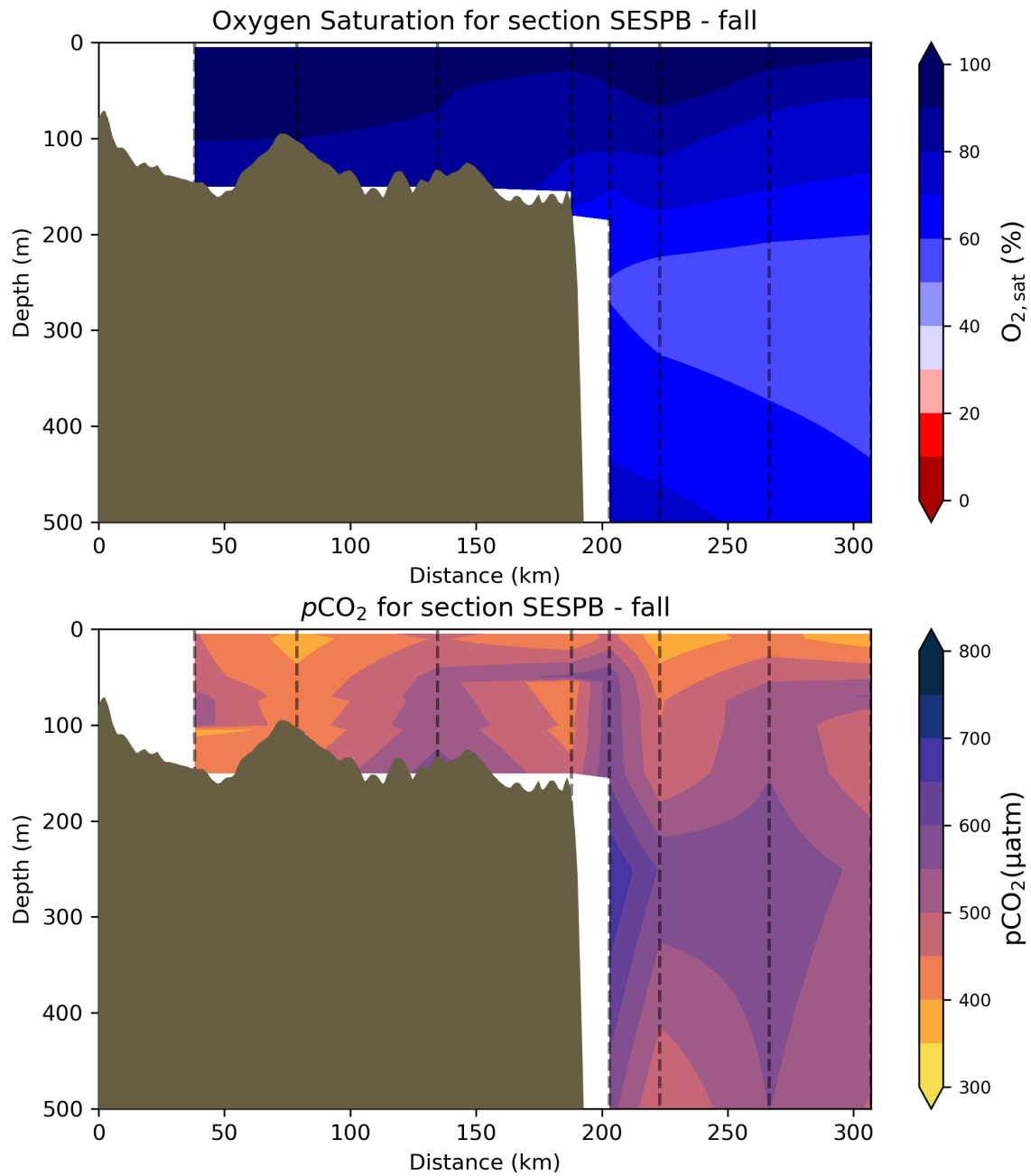
Figure 9. Depth-distance (x-axis is the distance in km from first station) contours along standard section Southeast St. Pierre Bank (SESPB) off the southern Newfoundland Slope (2015-2018 average). a) oxygen minimum and b) pCO$_2$. The dashed-lines represent to positions of the casts where the samples are collected.
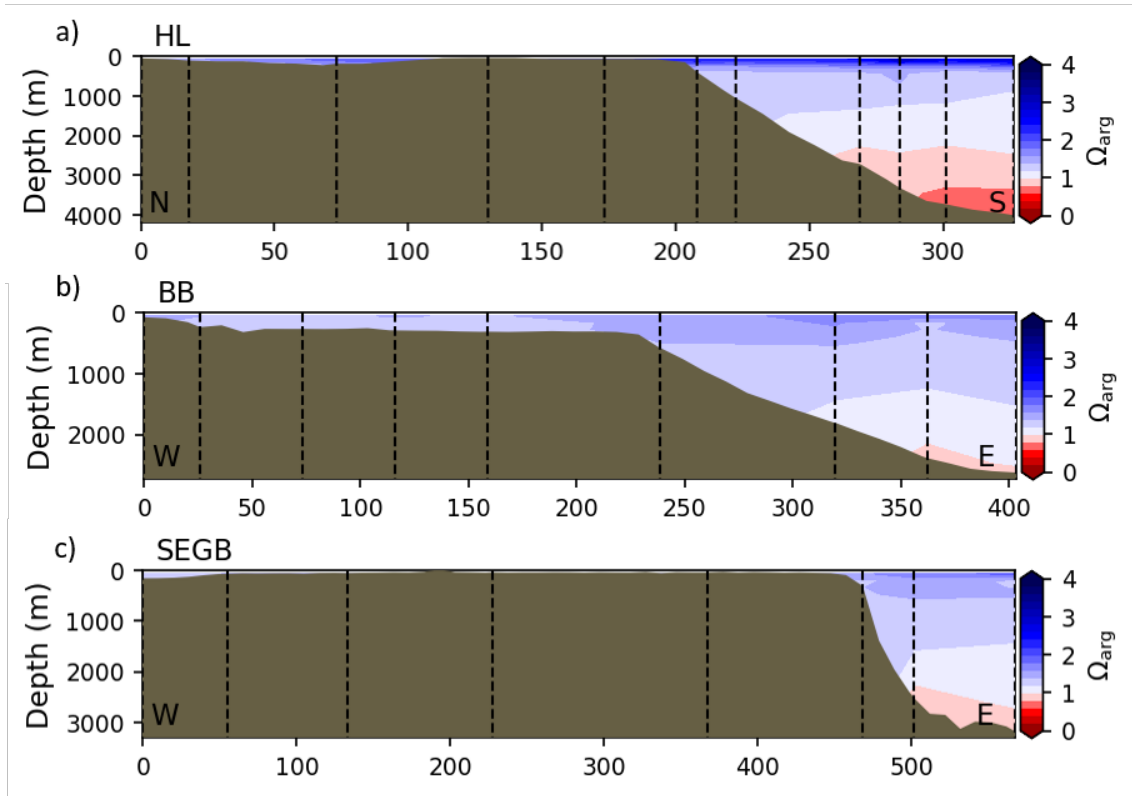
Figure 10. Depth profiles along standard sections in the Atlantic Zone for the fall of 2017. The aragonite saturation horizon ($\Omega_{\text{arg}} = 1$) is located between ~2200 and 2300 m along sections HL (a), BB (b), SEGB (c) above the Scotian and NL Slopes.

Appendix A: Seasonal maps of various parameters during 2017.

This Appendix presents a series of seasonal maps (spring, summer and fall) of various physico-chemical parameters collected as part of the AZMP during 2017, one of the most complete year of sampling. These parameters are: Temperature, Salinity, $O_{2_{sat}}$, TA, TIC, pCO_2, pH, Ω_{arg} and Ω_{cal}. They are presented in Figures A1 to A9, respectively. Each figure has 6 panels where the top row is the surface (upper most sample <52m) and the bottom row the near bottom (deepest sample >50m) conditions. The spring, summer and fall seasons are presented from left to right.

Appendix B: Hydrographic Sections

Figures A10 to A14 show contour plots of various physico-chemical parameters collected as part of the AZMP (the same as in Appendix A) along selected hydrographic sections of the Atlantic Zone during the fall of 2017 (see Figure 3 for location). These sections are Seal Island (SI), Flemish cap (FC), Halifax (HL), Cabot Strait (CSL) and Laurentian Channel (LC) and are presented in Figures A10 to A14, respectively. Each figure shows, from top to bottom panels, the Temperature, Salinity, $O_{2_{sat}}$, TA, TIC, pCO_2, pH, Ω_{arg} and Ω_{cal}, respectively.
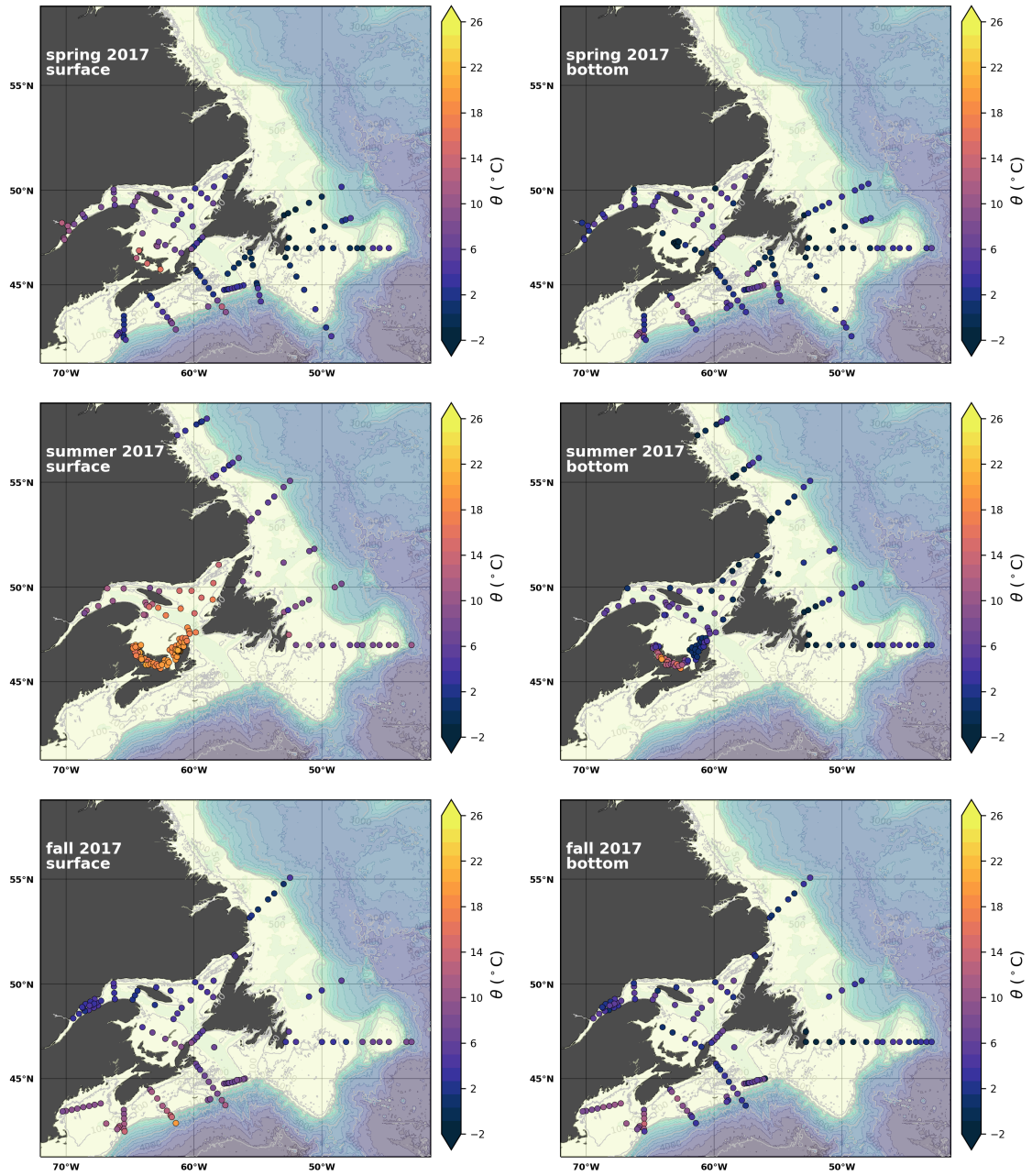
Figure A1. Surface (upper most sample <52m; top row), and near-bottom (deepest sample >50m; bottom row) temperature sampled during the spring (left), summer (middle) and fall (right) AZMP surveys.
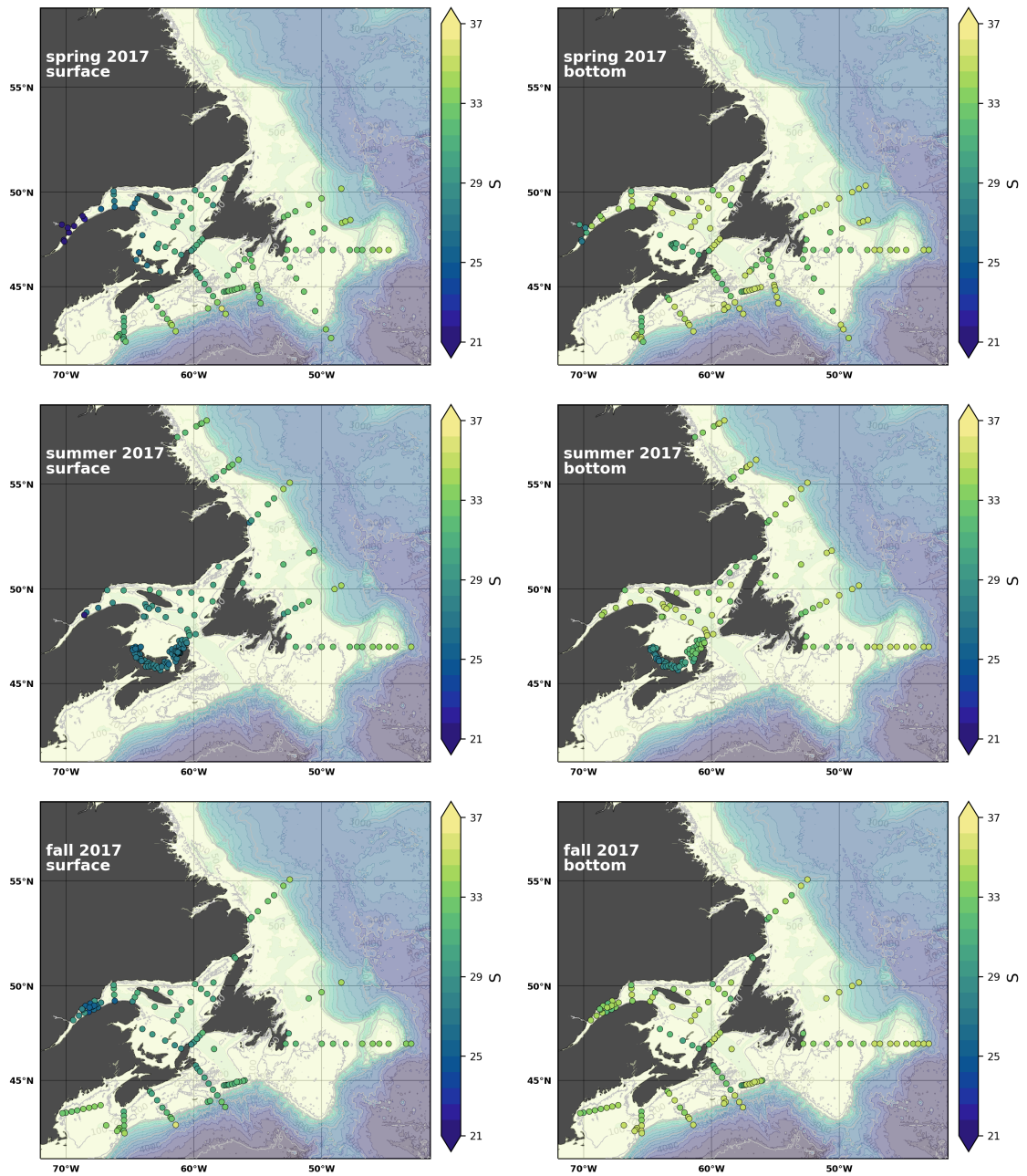
Figure A2. Same as in Figure A1, but for salinity.
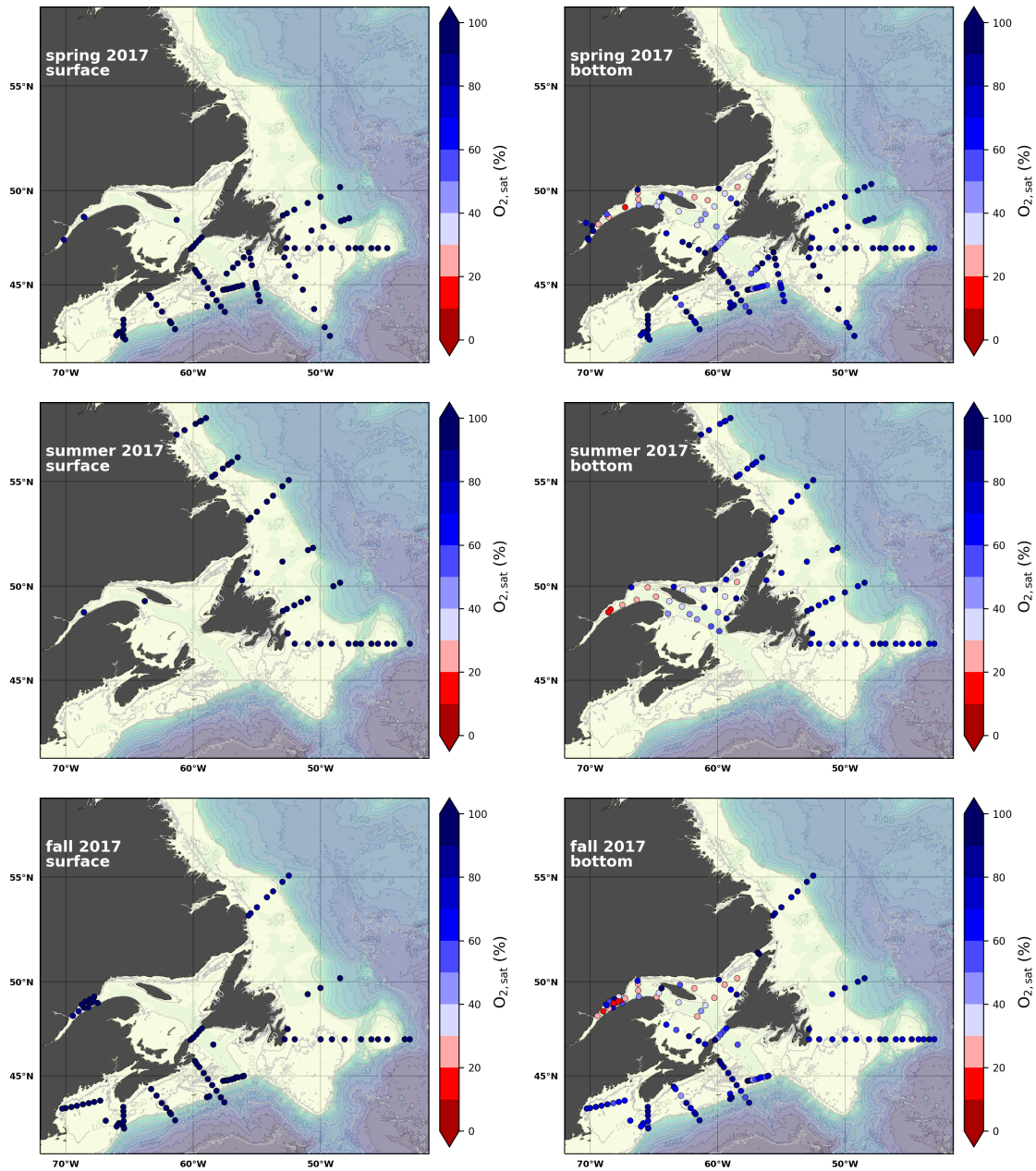
Figure A3. Same as in Figure A1, but for $O_{2_{sat}}$.
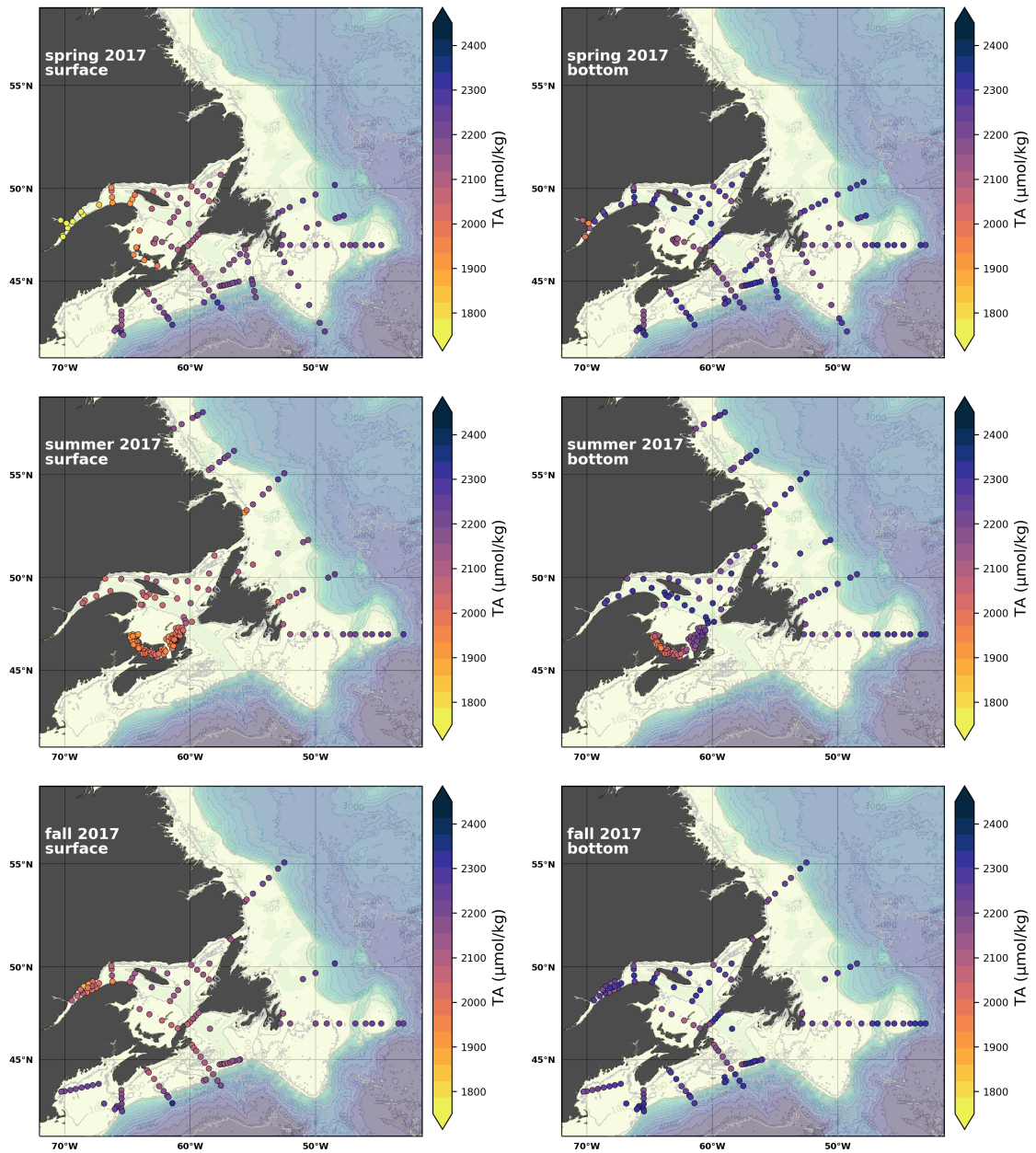
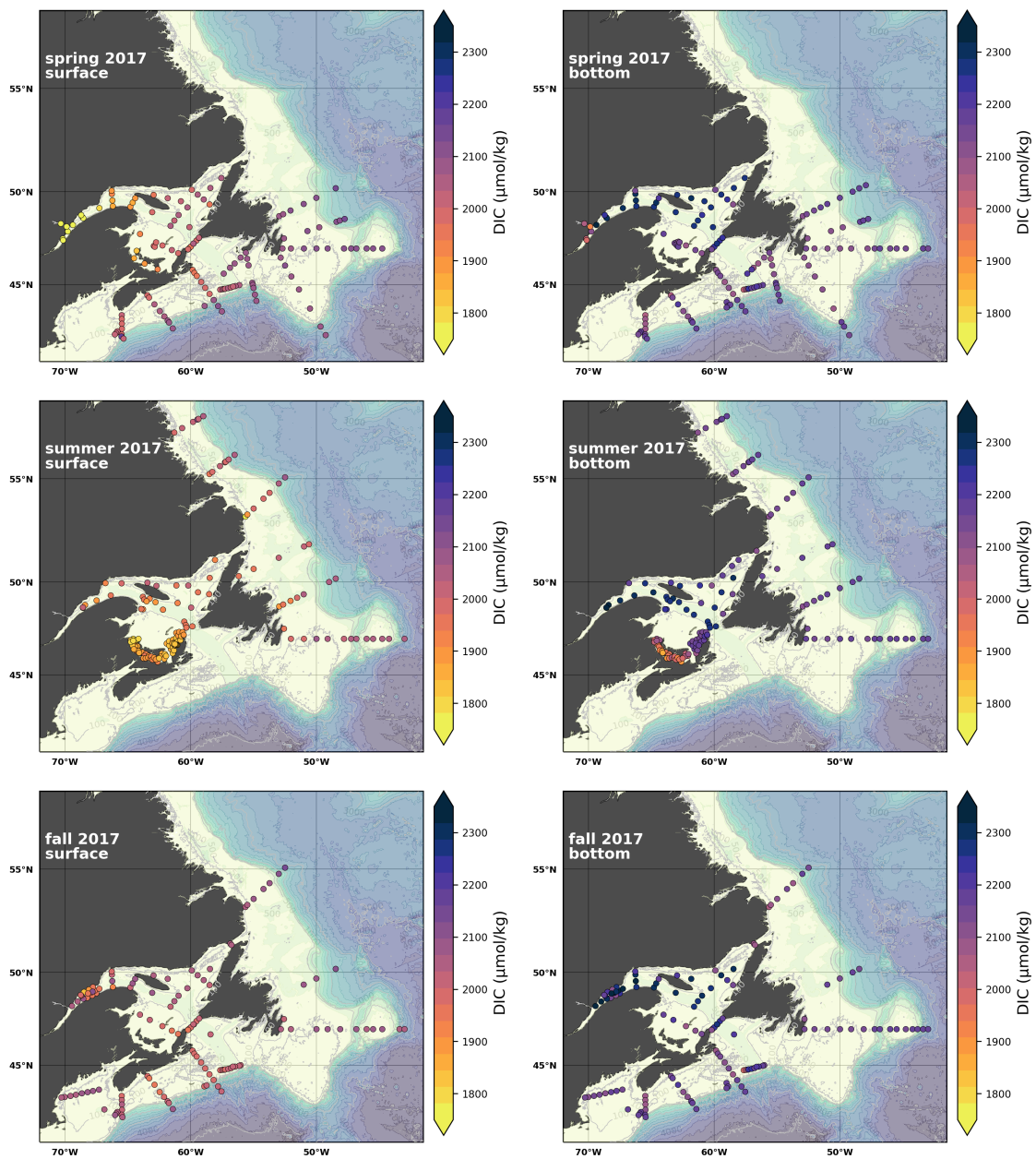**Figure A4.** Same as in Figure A1, but for TA.
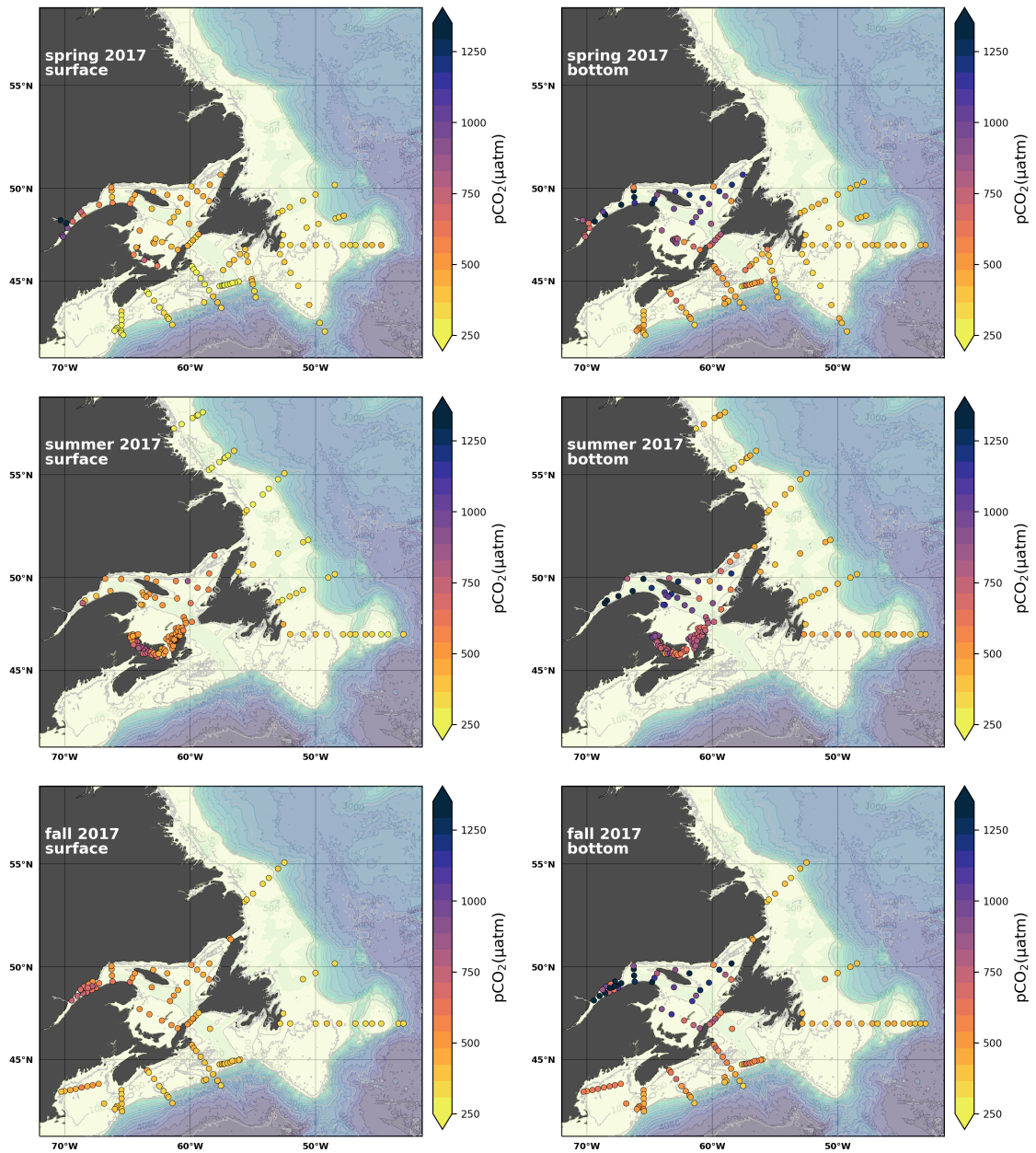
Figure A5. Same as in Figure A1, but for TIC.
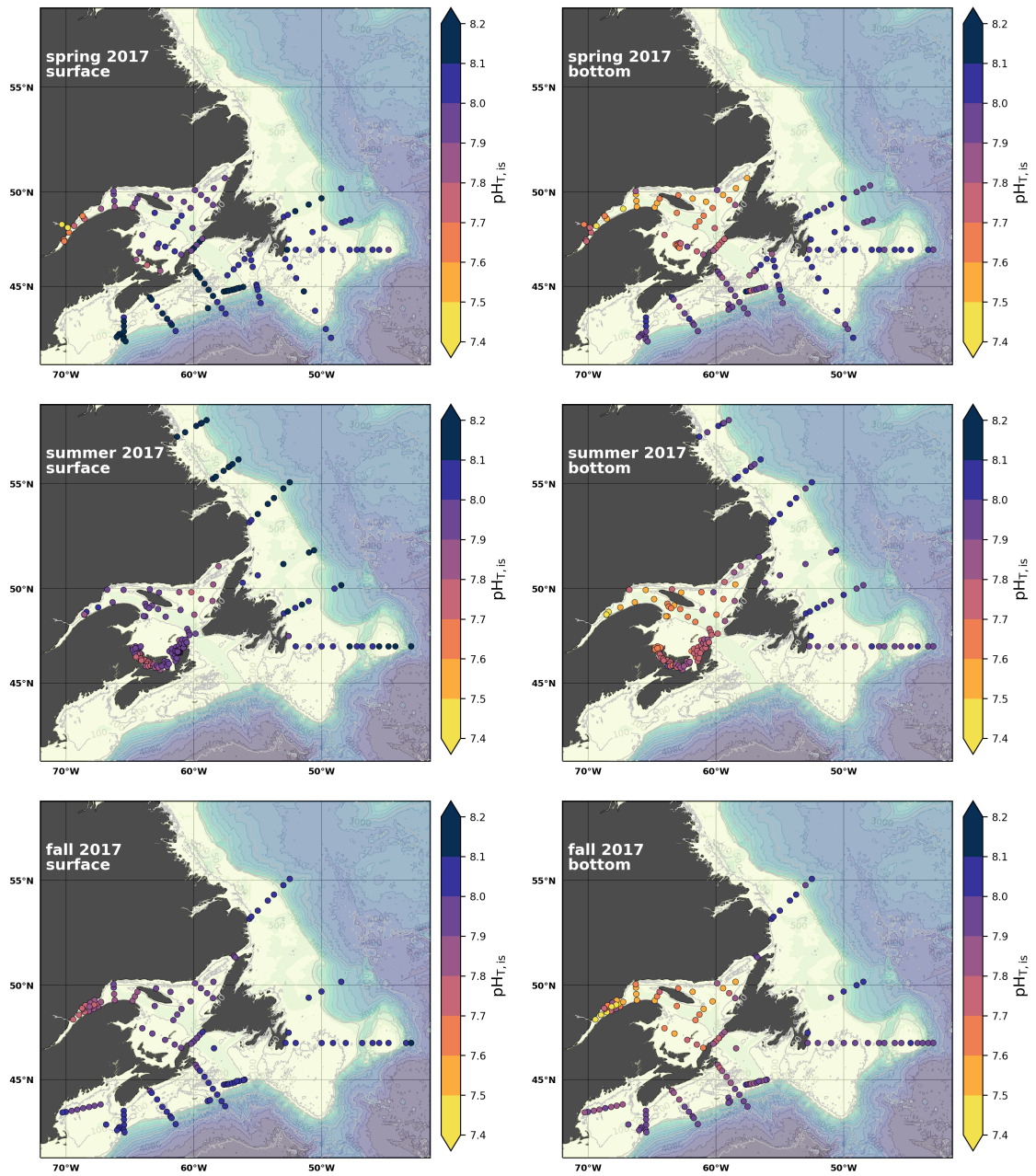
Figure A6. Same as in Figure A1, but for $p\text{CO}_2$

Figure A7. Same as in Figure A1, but for pH.
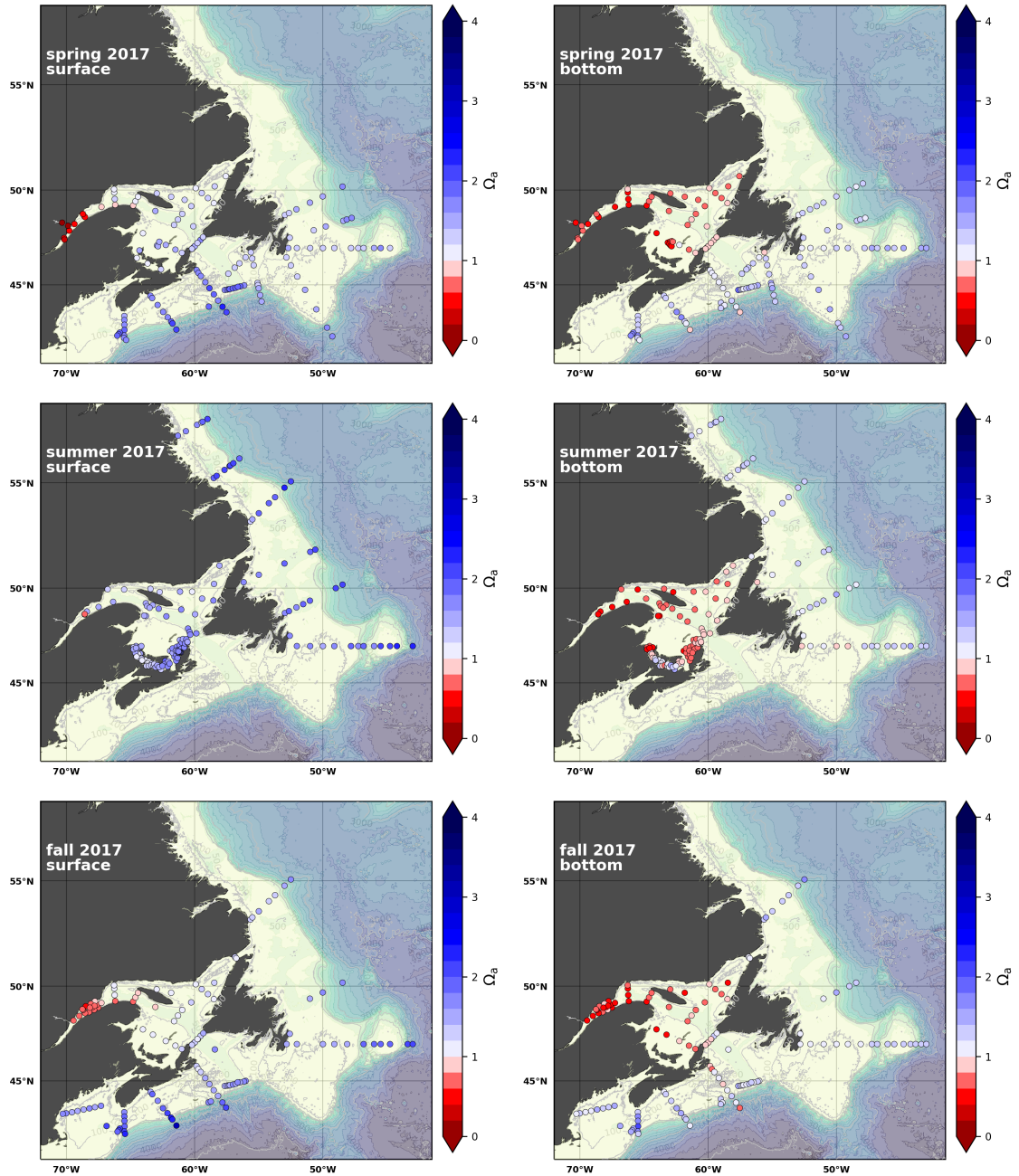
Figure A8. Same as in Figure A1, but for Ω_{arg}.
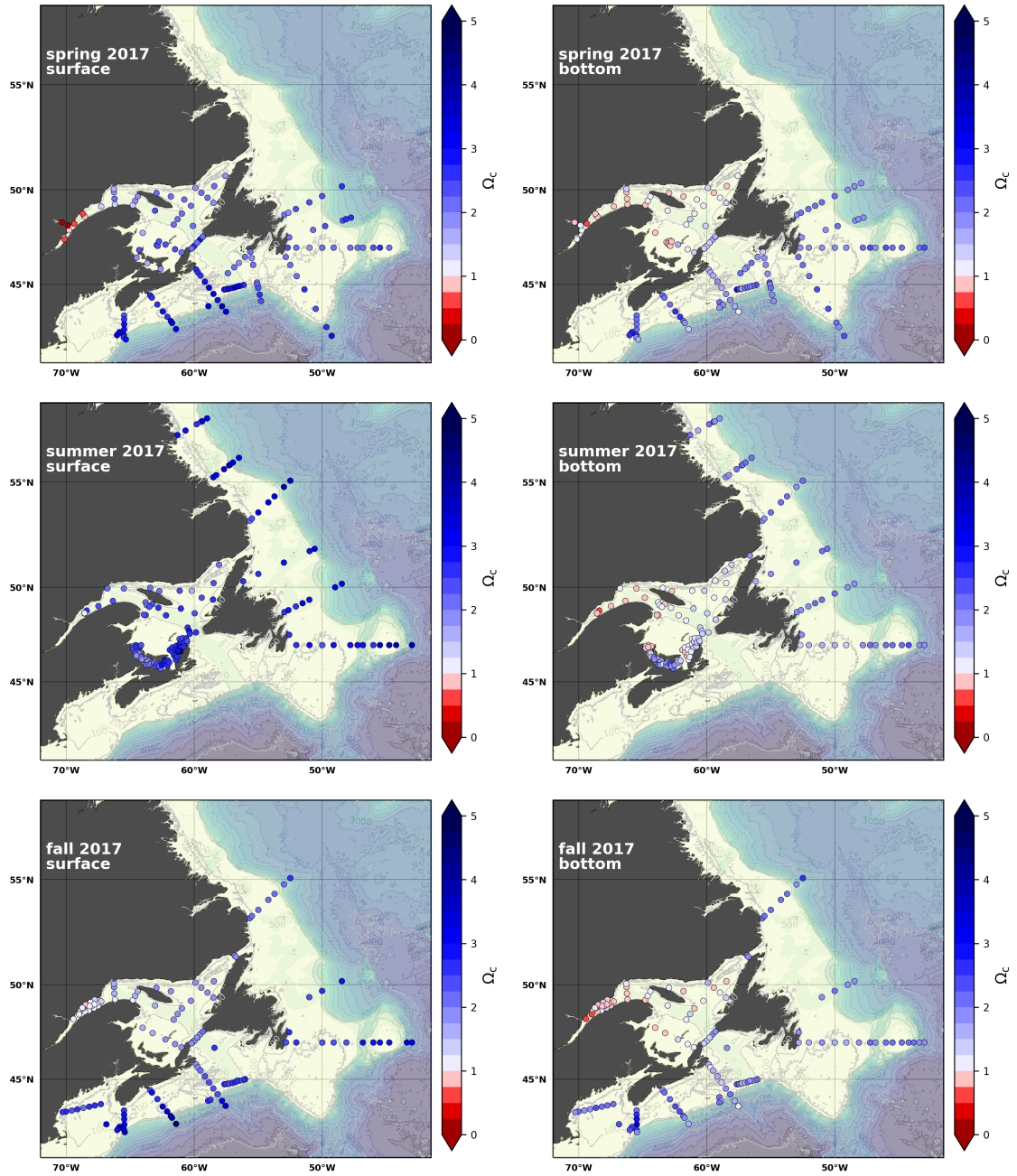
Figure A9. Same as in Figure A1, but for Ω_{cal}.
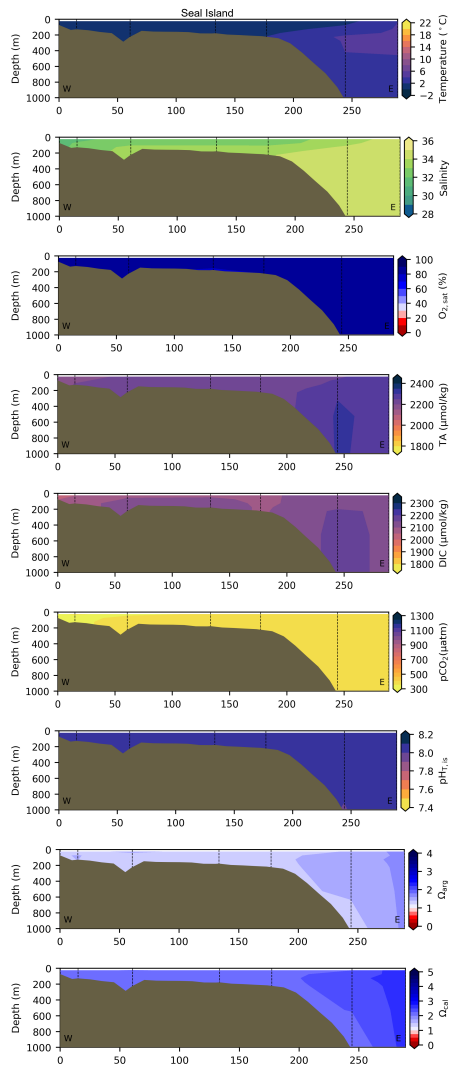
Figure A10. Contour plots of various physico-chemical parameters collected during the fall 2017 AZMP survey along hydrographic section Seal Island (NL region, see Figure 3 for location). From top to bottom, these parameters are respectively: Temperature, Salinity, O_{2_sat}, TA, TIC, $p\text{CO}_2$, pH, Ω_arg and Ω_cal.
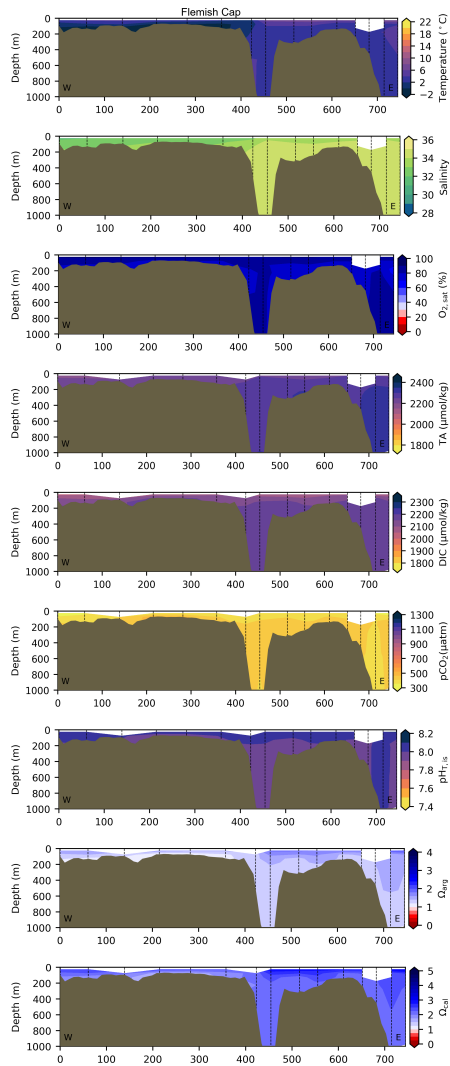
Figure A11. Same as in Figure A10, but for hydrographic section Flemish Cap (NL region, see Figure 3 for location).
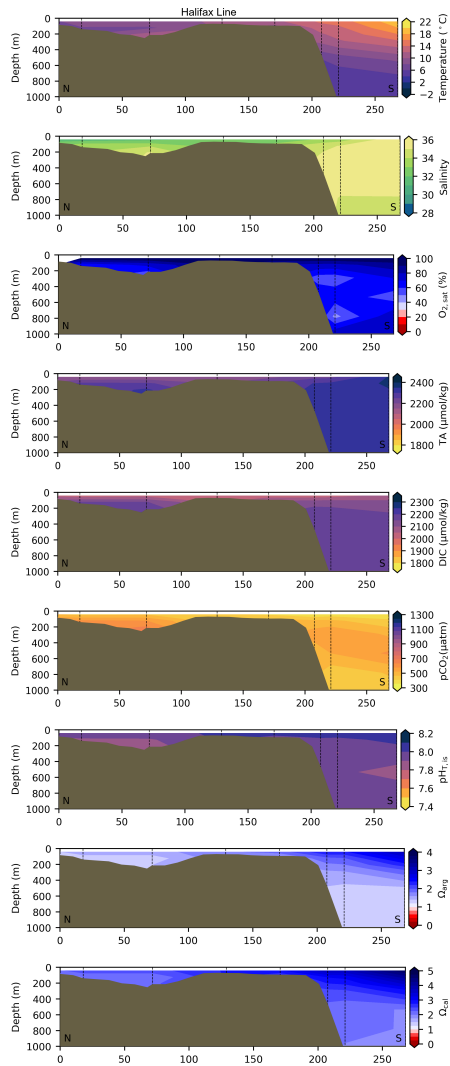
Figure A12. Same as in Figure A10, but for hydrographic section Halifax (MAR region, see Figure 3 for location).
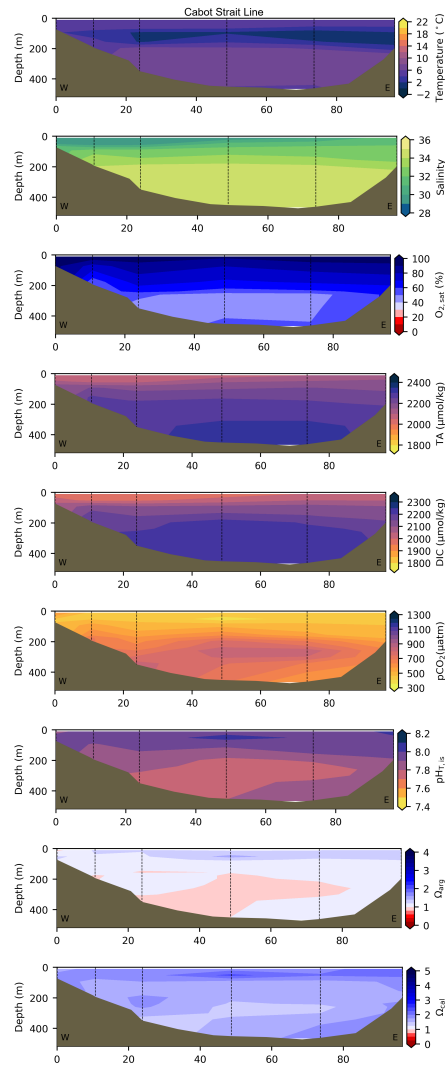
Figure A13. Same as in Figure A10, but for hydrographic section Cabot Strait (GSL region, see Figure 3 for location).
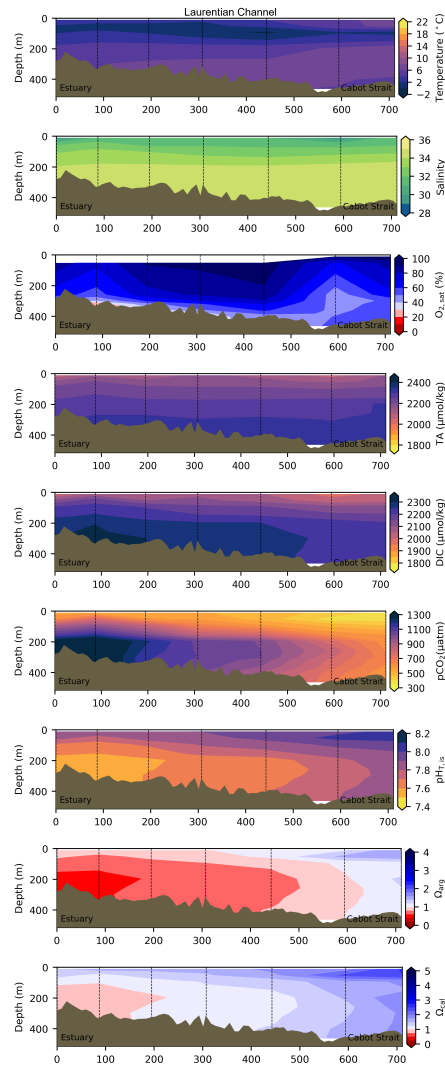
Figure A14. Same as in Figure A10, but for hydrographic section Laurentian Channel (GSL region, see Figure 3 for location).